

F. Meutzner^{1,2} / T. Nestler¹ / M. Zschornak^{1,3} / P. Canepa⁴ / G. S. Gautam⁵ / S. Leoni⁶ / S. Adams⁷ /
T. Leisegang^{1,2} / V. A. Blatov² / D. C. Meyer¹

Computational analysis and identification of battery materials

¹ TU Bergakademie Freiberg, Institut für Experimentelle Physik, Leipziger Str. 23, Freiberg 09596, Germany, E-mail: falk.meutzner@physik.tu-freiberg.de, tina.nestler@physik.tu-freiberg.de, matthias.zschornak@physik.tu-freiberg.de, tilmann.leisegang@physik.tu-freiberg.de, dirk-carl.meyer@physik.tu-freiberg.de

² Samara National Research University, Moskovskoye Shosse 34, Samara 443086, Russian Federation, E-mail: falk.meutzner@physik.tu-freiberg.de, tilmann.leisegang@physik.tu-freiberg.de, blatov@samsu.ru

³ Helmholtz-Zentrum Dresden-Rossendorf e.V. (HZDR), Institute of Ion Beam Physics & Materials Research, Bautzner Landstraße 400, Dresden 01328, Germany, E-mail: matthias.zschornak@physik.tu-freiberg.de

⁴ Department of Chemistry, University of Bath, Bath BA2 7AY, United Kingdom, E-mail: pcanepa@lbl.gov

⁵ Department of Mechanical and Aerospace Engineering, Princeton University, Princeton, NJ 08544, USA, E-mail: gautam91@princeton.edu

⁶ School of Chemistry, Cardiff University, Cardiff CF10 3AT, UK, E-mail: leonis@cf.ac.uk

⁷ Department of Materials Science & Engineering, National University of Singapore, Engineering Drive 2, 117579 Singapore, Singapore, E-mail: mseasn@nus.edu.sg

Abstract:

Crystallography is a powerful descriptor of the atomic structure of solid-state matter and can be applied to analyse the phenomena present in functional materials. Especially for ion diffusion – one of the main processes found in electrochemical energy storage materials – crystallography can describe and evaluate the elementary steps for the hopping of mobile species from one crystallographic site to another. By translating this knowledge into parameters and search for similar numbers in other materials, promising compounds for future energy storage materials can be identified. Large crystal structure databases like the ICSD, CSD, and PCD have accumulated millions of measured crystal structures and thus represent valuable sources for future data mining and big-data approaches. In this work we want to present, on the one hand, crystallographic approaches based on geometric and crystal-chemical descriptors that can be easily applied to very large databases. On the other hand, we want to show methodologies based on *ab initio* and electronic modelling which can simulate the structure features more realistically, incorporating also dynamic processes. Their theoretical background, applicability, and selected examples are presented.

Keywords: crystallography, electrochemistry, Voronoi–Dirichlet partitioning, bond valence sum, density functional theory

DOI: 10.1515/psr-2018-0044

1 Introduction

The exponential growth of computer-processing power described by the empirical “Moore’s Law”, formulated in 1965 by Gordon Moore, has led to increasingly faster processors. This enabled powerful and very diverse computational methods including algorithms with a higher demand of computational power. They are becoming widely used today for tackling problems in materials science and engineering. Big-data approaches as well as multiphysics modelling employing finite elements all the way to quantum mechanical modelling can nowadays virtually simulate and test thousands of materials at a time. In science as well as in industry, these methods are becoming increasingly important to predict functional materials with enhanced properties: In Ref. [1], Ceder and Persson state that “yet materials science is on the verge of a revolution”. With respect to the development and discovery of new battery materials, computational methods are becoming a main driver. Hence, they will be a key enabler for the storage of large amounts of renewable energies and thus its further installation, since low cost and durable systems with preferably higher energy densities are needed. In order to use the potential to develop materials for ground-breaking technologies, the availability of infrastructure for High-Performance Computing (HPC) is the key factor [2]. In 2011, the Materials Genome Initiative (MGI) was

F. Meutzner is the corresponding author.
© 2018 Walter de Gruyter GmbH, Berlin/Boston.

established in the US, promising a renaissance of the American manufacturing industry by at least doubling the pace of discovery, development, and deployment of new materials so that they are introduced to the market at a fraction of the cost [3]. Several other national computing clusters as well as the Partnership for Advanced Computing in Europe (PRACE) has thus been founded or extended in recent years in order to offer computing and data management resources and services [2, 4–6].

In former days, the only way to find and explore new materials was to synthesise and test an enormous amount of different compounds based on the researcher's experience [7].¹ Once a variety of successful compounds and structures has been found by this trial-and-error-technique, advanced materials can be accessed by atomic substitution or doping. Even though material engineering can, for instance, be performed by experimental high-throughput combinatorial screening nowadays [8, 9], this approach is still extremely time-consuming and will rather lead to evolutionary than revolutionary findings. Additionally, the hope to be able to transfer compounds or at least structural motifs from the lithium-ion-battery to high-valent² battery materials such as magnesium [10] and aluminium [11] often failed, demonstrating the need to start from scratch.

A more time-efficient route would rather be to employ computational methods. They are already powerful enough to eliminate significant parts of the guesswork, as they can predict many properties relevant for battery materials before they are synthesised in the lab. For instance, by scaling material computations over supercomputing clusters [4], Ceder's group has predicted several new battery materials, which were then synthesised and tested in the lab. For instance, on this basis, Pellion Technologies was founded for the development and commercialisation of high-energy-density rechargeable magnesium-ion batteries for applications that range from portable electronics to electrified vehicles [12, 13].

Besides the design and evaluation of new compounds, the search among already known materials by means of high-throughput theoretical methods appears highly promising, since for example the most successful cathode materials for lithium-ion batteries have been known for years, before they were considered and validated for the use in batteries.³ This fact motivated several studies to screen structural databases such as the Inorganic Crystal Structure Database (ICSD) for new battery materials and already lead to new discoveries of such compounds (e.g. [14–19]). Furthermore, in combination with already established or future available experimental characteristics, the data created during the screening process can lead to a deeper insight into the fundamental relationship between the structure and functional properties of battery materials (e.g. shown in [20, 21]), which helps to optimise and design the next generation of battery materials.

Based on preliminary data mining, the setting up of structure-property relations is a valuable productive approach commonly used in crystallography and materials science. According to Merriam-Webster [22], *data mining* is described as "the practice of searching through large amounts of computerised data to find useful patterns or trends", using pattern recognition technologies as well as statistical and mathematical techniques (see [23] for details). Eventually, by applying the outcome of continuing data mining in an iterating way, the so-called *machine-learning* is achieved, which will decisively accelerate our knowledge growth [24]. Nowadays, databases are increasing in size and complexity, eventually even coining the term *big data*, which is stated to become a key basis of competition, productivity growth, innovation, and consumer surplus [25]. For instance, the collection of data thus allows drawing conclusions from materials with the same function but very different crystallographic structures. The more data is generated and analysed, the more reliable the results become and the more reliable predictions can be derived utilising this data. By applying the knowledge gained through data mining, different data sets may be identified that comprise compounds with the same functionality but have not yet been analysed for it.

Several examples based on data mining for targeting battery materials are known: electrolytes [19, 26, 27], cathodes [4, 28], and electrodes (chapter "Material assessment"). Besides battery materials and in particular the "Materials Project" [4], other projects and initiatives (see in Ref. [9]) also make use of this approach: the Harvard Clean Energy Project [29], which has focused on photovoltaic materials, AFLOWlib [30], which addresses the electronic structure of inorganic compounds to uncover thermoelectric and scintillator materials as well as magnetic materials for energy and spintronics applications, and OQMD, which specialises in thermodynamic properties [31]. These screenings target different material properties and apply diverse methods. An overview on the figures of merit that can be evaluated today for electrodes and electrolytes and the corresponding applicable theoretical methods is given in Figure 1.

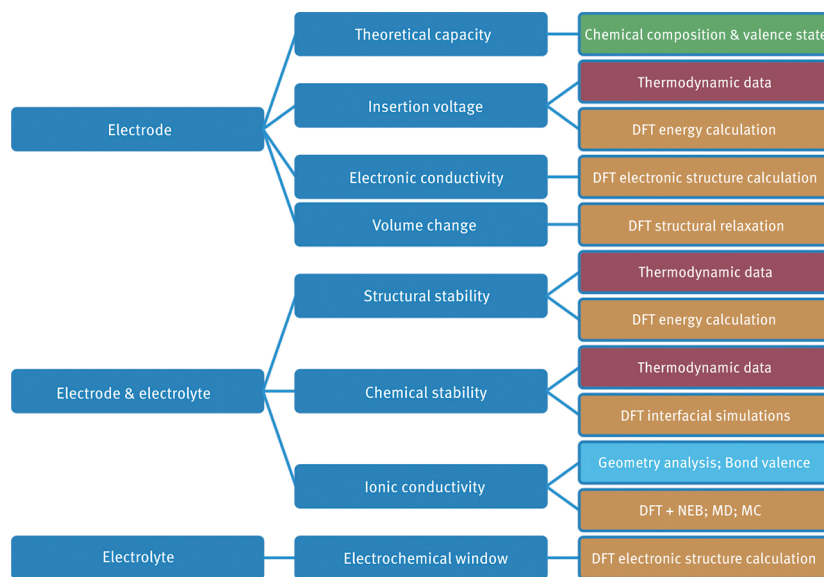


Figure 1: Relevant properties to forecast the performance of electrode and electrolyte materials that can be simulated, and theoretical methods used to calculate them (DFT: density functional theory, NEB: nudged elastic band, MD: molecular dynamic; MC: Monte Carlo). Scheme was adapted from Ref. [35].

For instance, to select candidates for new solid electrolytes, high ionic conductivity is the most important criterion besides structural and electrochemical stability. For insertion-type electrode materials, the ionic conductivity in the electrodes limits the rate capability [21]. Typically, a balance has to be found between these, as high ion mobility also tends to reduce the structural stability. Precise simulations of migration barriers with density functional theory (DFT) employing the nudged elastic band (NEB) method [32] for thousands of structures, however, would take years or even decades. Even then, the migration barriers will only allow for a rough prediction of the absolute room temperature conductivities, which strongly depend on the often non-equilibrated defect concentrations and distributions in real materials. Practically, the reliability of DFT predictions also depends on whether all potentially relevant ion migration pathways, e.g. those between nominally unoccupied sites, have been included in the considerations. Direct screening of the ion dynamics by *ab initio* molecular dynamics (MD) simulations at relevant temperatures still appears out of reach and will anyways not solve the problems of defect influences. For polycrystalline materials, the microstructure often limits the practically achievable conductivity. This, as well as the lower variability of entropy in strongly disordered glasses, contributes to the finding that the prediction of absolute conductivities from local structure models via a determination of migration barriers is more reliable for glasses than for crystalline compounds [33].

Since the significantly higher effort in determining migration barriers by DFT cannot ensure a significantly more precise prediction of absolute conductivities anyways, some studies undertake computationally less expensive and intrinsically less accurate estimations of the migration barriers first, such as the geometry-based Voronoi-Dirichlet Partitioning [19] or bond valence sum (BVS) methods [34–36], like bond valence site energies (BVSE) [16, 37–39], where part of the saved computational cost can be spent on treating more complex local structure models and on ensuring that no pathway is overlooked. Further methods comprise e.g., Hirshfeld and procrystal analysis [40, 41].

It has to be noted, however, that the applicability and forecasting power of these methods is generally limited in comparison to DFT and in particular to dynamic approaches such as MD and Monte Carlo (MC) simulations. Voronoi-Dirichlet partitioning and BVS, or BVSE, are not applicable to alloys and in order to utilise them for other amorphous compounds, a representative local structure model of the amorphous materials has to be generated first. Since this involves rather time-consuming methods such as Reverse MC fitting of neutron and synchrotron diffraction data [42–45], a screening of amorphous materials appears not feasible yet. Additionally, all the listed approaches only simulate on an atomic or molecular scale. In order to realistically predict the material's performance in the battery, other so-called multiscale techniques are needed in the future, which incorporate microstructural defects and describe the interplay between the individual materials and the electrical and physical behaviour of the cell as a whole. One example for a possible algorithm is the application of finite element methods as implemented for example in Comsol's multiphysics programme [46–48]. By inputting a number of physical and chemical parameters, the operating cell can be simulated. On the other hand, with respect to thiophosphate-based solid electrolytes in lithium all-solid-state batteries, the bulk ion conductivity is not rate limiting anymore. In fact, the grain boundary resistance as well as the interface resistance to the electrode dominates the cell performance ([49], for a theoretical description see chapter "Separators and solid

electrolytes" of [50]). However, it is not possible to take these phenomena into account by screening methods, yet, since we are just on the way to fully understand and describe them.

Besides the typical criteria for good electrodes and electrolytes, which are discussed in the chapter "Separators and solid electrolytes" of [50], the simulation of the volume change is of interest in the case of insertion or phase transition electrodes. A small volume change is generally related to a longer cycle life of lithium-ion batteries [51] and even more important for the improvement of all-solid-state batteries.

To sum up, the use of computational methods, in particular high-throughput technologies and big-data approaches, appears promising for identifying and simulating materials with dedicated or novel properties in order to realise new concepts for electrochemical energy storage. This review gives an overview about relevant methods developed for deepening the understanding of and finding novel battery materials. The presented approaches can be applied for both predicting the properties of a specific compound and screening structure databases for potential battery materials. They cover the simulation of different properties and also different accuracy levels and thus computational effort. For the screening of crystalline solid electrolytes and intercalation materials, the authors thus suggest using these methods in succession in order to build a "filter"; that means e.g. first Voronoi-Dirichlet Partitioning, followed by BV-based methods and finally DFT and MD (Figure 2). Promising candidates are picked out first to be evaluated more precisely with increasingly time-consuming but more accurate methods. This sequential use thus allows a fast approach to reliably screen thousands of compounds. In the following, the respective methodologies are presented and their features and characteristics are highlighted.

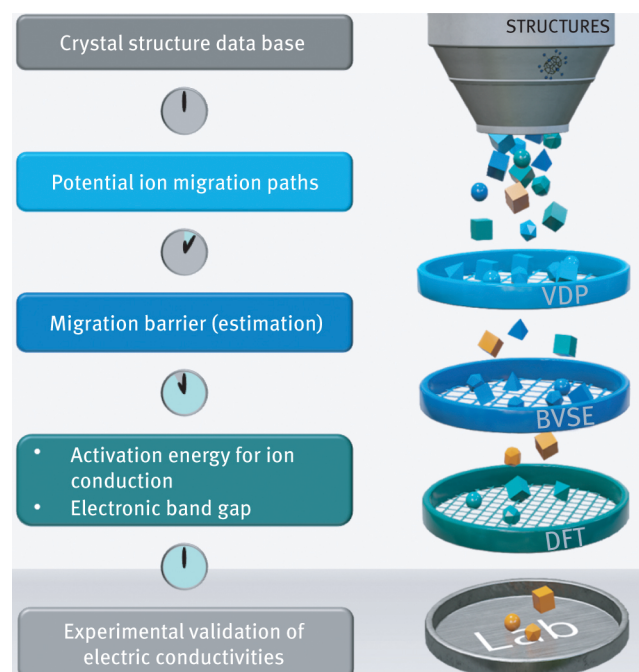


Figure 2: Scheme of the suggested screening approach for crystalline materials with fast ionic transport. Simulation methods with different accuracy levels and thus computational effort, as indicated by the clock symbol, are performed in succession.

2 Voronoi-Dirichlet partitioning

2.1 Introduction

The classic description of crystallography focuses on space groups and embedded atoms on Wyckoff sites. Since its introduction, many different descriptions have been presented in the crystallographic literature, that is e.g. the assignment of a three-dimensional periodic arrangement of atoms to a unit cell belonging to one of the 230 space groups [52], the determination of the chemical topology as independent one-, two-, and three-dimensional interpenetrating nets [53–55], or the partitioning of the atomic environments by coordination polyhedra or clusters, e.g. Frank-Kasper and other polyhedra [56–59]. Thus, atomic arrangements can be analysed from a solely geometric point-of-view. Comparing the arrangement of bonded atoms in thousands of existing compounds, geometrical and topological analyses reveal relationships – recurring structural motifs – between numerous crystal structures even though they may not be directly related from a space group point-of-view.

In crystal chemistry, atoms are usually described as hard spheres or point-like objects that are positioned in a 3D space. Therefore, these atomic arrangements can be geometrically understood as point arrangements in space. Voronoi diagrams or Dirichlet domains have been widely used in geometrical analyses to describe the relationships and domains of single points in point arrangements. Especially in computer algorithms for the retrieval of data in databases, collision control, and the analysis of clustering, Voronoi diagrams have been extensively used. Further applications are e.g. described by Aurenhammer [60].

The polyhedron created through Voronoi-Dirichlet partitioning is called “Voronoi-Dirichlet polyhedron” (VDP) [61, 62] and has been interpreted crystal-chemically since 1927 [63], with interest intensifying since around 1995 [64, 65]. Voronoi-Dirichlet partitioning geometrically subdivides a space filled with points (atoms). This VDP is generated⁴ for a given point i (the central point) in an assembly of its n neighbouring points j by constructing planes perpendicular to and midway on all line segments ij that connect the central point to all other points. The smallest polyhedron created in this way is the VDP of the point i . Therefore, the VDP pinpoints towards the nearest neighbours of a point because the planes created between close points are closest to the central point. Each additional point that lies inside this construct is closer to point i than to any other point j . Figure 3 shows a two-dimensional representation of the VDP. For atomic structures, each point is identified with an atom or ion (for the sake of readability, the terms atom and ion will be subsumed to a generic atom). These polyhedra therefore describe a certain volume (or domain) in a structure that can be assigned to a certain atom, as each point in this domain is closer to this atom than to any other atom (Figure 3). The idea of these *domains of action* (“Wirkungsbereiche”) was already proposed by Niggli in 1927 and lays thus the foundation of topological crystal chemistry [63]. For periodic real space lattices, the VDP is thus equivalent to the Wigner-Seitz elementary cell and the application of the same construction method to reciprocal lattices yields the first Brillouin zone. More details of the history and the development of Voronoi-Dirichlet partitioning, which can in its simplest form be traced back to René Descartes’ work [66], can be found in [65, 67, 68]. The following sections will subsume and refer to many of the authors’ findings already published in Refs [19, 27].

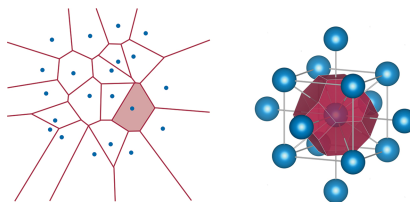


Figure 3: Left-hand side: two-dimensional representation of a Voronoi diagram. Segments between each blue dot are drawn and in the middle, a perpendicular line is constructed. The smallest polyhedron created around a given reference dot is its Voronoi-Dirichlet polyhedron (e.g. the area shaded in red). This figure was created with [69]. Right-hand side: Construction of a VDP for a body-centred cubic structure (blue atoms) with the corresponding vertices (grey) that signify voids in the structure.

2.2 The Voronoi-Dirichlet approach

The Voronoi-Dirichlet approach, carried out with the programme package “ToposPro” as described in [27, 54, 70], is a sophisticated crystal-chemically motivated and geometrically performed, high-throughput crystallographic analysis that can be easily applied to large crystal structure databases. The VDP of an atom in a structure is characterised by its volume, faces, vertices, and edges [65]. Volumes can be used to describe the size and shape of this atom in the crystal structure in the case of homogeneous environment of an atom (e.g. oxygen environment of metal atoms in oxides). The size of a face of a VDP is proportional to the strength of the chemical bonding to a neighbouring atom for a given atomic pair (e.g. cation-anion like Mg^{2+} and O^{2-}). The closer a neighbour, the larger a face and the higher the attractive force between the central atom and its neighbour and thus the stronger the bond. By finding the atoms that share the largest faces of a VDP, the nearest neighbours are identified. According to Ref. [65], the face sizes can also be described by solid angles Ω – specifying the percentage of the face projected onto a unit sphere. The vertices of a VDP describe possible voids in the structure because they are farthest away from all surrounding atoms. Each vertex is connected to neighbouring vertices through VDP edges. These edges are, in analogy to the vertices, the farthest away from their constructing atoms. They can thus be regarded as channels between these voids (see Figure 3 and Figure 4).

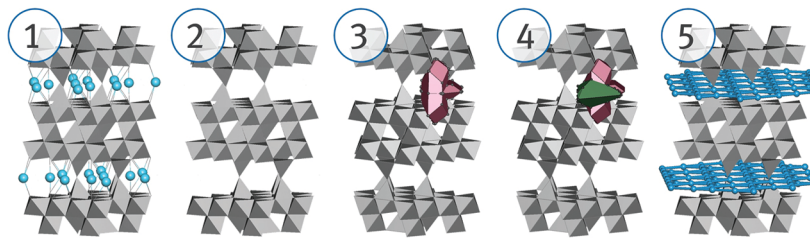


Figure 4: Graphical demonstration of the Voronoi-Dirichlet approach applied to Na β -alumina (ICSD-# 9144). From the structure (1) all Na-ions (light blue) are ignored (2) and the VDP of all remaining atomic sites (selection in red) are calculated (3). For each of these VDPs vertices, a further VDP (green) is constructed (4) and compared to data-mined values in order to generate the conduction path (blue) (5). Figure reproduced with permission from [F. Meutzner, W. Münchgesang, T. Leisegang, R. Schmid, M. Zschornak, M. Ureña de Vivanco, A. P. Shevchenko, V. A. Blatov, and D. C. Meyer: "Identification of solid oxygen-containing Na-electrolytes: An assessment based on crystallographic and economic parameters", *Crystal Research and Technology* 52, 1600223 (2017).], © 2016 WILEY-VCH Verlag GmbH & Co. KGaA, Weinheim.

By constructing secondary VDP for each single vertex of the primary VDP and the respective surrounding atoms, the space that is assigned to this vertex/void can be determined. Thus, atoms can be identified that could theoretically occupy this space. If neighbouring voids can host the same atom, there will be a VDP edge connecting them. By analysing the space between the constituting atoms, the edge can be evaluated as a potential diffusion path between these two voids. Also, a tertiary VDP can be used in the channel to determine the passage size of a migrating ion, allowing a more generalised description of migration space for mobile ions.

The information-analytical system "ToposPro" is used for constructing VDP. It is a multifunctional tool for crystallographic analysis, which enables the application of VDP analysis and special topological methods for crystal structures and whole crystallographic databases through built-in database-handling routines [54, 71]. ToposPro is designed to process long lists of crystal structures in batch mode, perform statistical analysis of the structural descriptors, and find relations between crystal structures of different chemical composition and complexity. It also allows the user to compute a number of topological parameters of crystal structures and store the values of various geometrical and topological characteristics, i.e. structure descriptors, in knowledge databases. For the analysis of ionic conductivity, the most important values are r_{SD} , G_3 , and r_{Chan} , as well as the solid angles of the void- and edge-constituting atoms [14, 70]. r_{SD} is the radius of a spherical domain that has the same volume as the considered VDP, which is a measure of the atomic size in the structure. G_3 is the second moment of inertia of the VDP, which is a measure for the sphericity of the VDP; the smaller this value, the more spherical the VDP [65]. r_{Chan} is the channel radius and describes the width of the bottleneck between two voids.

Additional special software enables to find the correlations between these descriptors and other structural properties, including physical properties using the statistical methods of regression and multifactor analysis. It also includes algorithms for the heuristic analysis and modelling of physical properties of substances (ionic conductivity, volatility) and allows for searching for structural relationships at different levels of the crystal organisation. ToposPro⁵ is an integrated interactive software environment functioning in the Windows operating system. The algorithms used in ToposPro are copyrighted by the Samara Centre for Theoretical Materials Science (SCTMS) and based on the theoretical models of graph and polyhedral representations of atoms, molecules, and compounds.

As described in [27], intercalation as a topochemical reaction can be easily described as the addition of an ion on an empty or partially occupied crystallographic site. The host structure stays more or less unchanged during insertion and removal of the intercalated species. For the whole crystal to accommodate a maximum number of ions, diffusion between these sites needs to be possible. In this way, crystalline solid ionic conductors can be described similarly to intercalation hosts. This idea is the basis of the application of the Voronoi-Dirichlet approach to describe and find new solid electrolytes [70]; it has been applied for Li-ion as well as Na-ion conducting oxides [14, 19, 27]. Based solely on geometry, it offers a very fast algorithm and allows the analysis of thousands of compounds within an hour regarding possible voids, their sizes and connections, and the resulting topology of the potential conduction network.

The most important factor for both voids and channels is their significance, which is connected to two conditions [70]:

1. Determination: In the case of cationic conduction, both voids and channels need to be determined only by anions. If one of the constituting atoms is a cation, Coulomb repulsion will give an energy barrier too large for another cation to enter this site or channel.
2. Comparison: The geometrical data of the voids and channels is compared to a set of expected values. That is, r_{SD} and G_3 need to be at least as large as/smaller than the data-mined values for the mobile ion in

question and its environment, respectively. For the channel radius, data-mined average distances need to be considered.

All the important steps for this methodology, including future testing of the newly identified materials, are summarised in Figure 5.

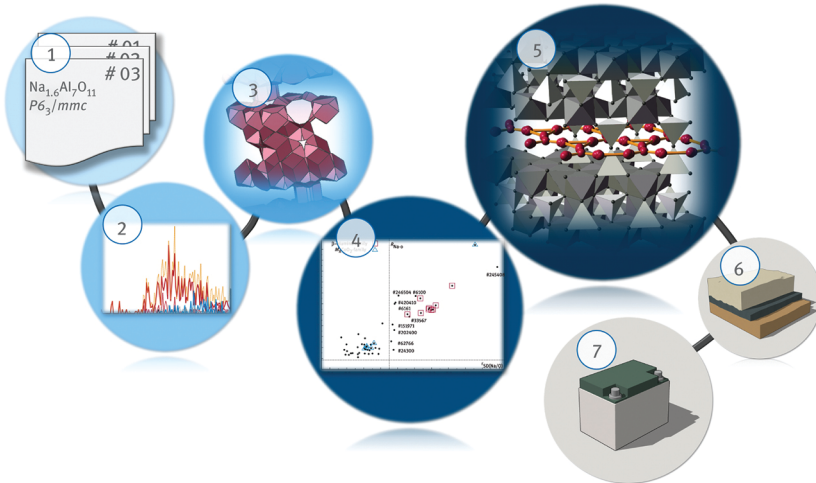


Figure 5: Graphical summary of all necessary steps for the Voronoi-Dirichlet approach. The starting point is the use of a database (1) for data mining (2). The Voronoi-Dirichlet partitioning (3) is then applied and the data-mined values (4) are applied to determine potential ion conductors/intercalation hosts (5). Experimental work (6) should finally clarify if the material qualifies for electrochemical storage technology (7). Figure reproduced with permission from [F. Meutzner, W. Münchgesang, N. A. Kabanova, M. Zschornak, T. Leisegang, V. A. Blatov, and D. C. Meyer: 'On the Way to New Possible Na-Ion Conductors: The Voronoi-Dirichlet Approach, Data Mining and Symmetry Considerations in Ternary Na Oxides', *Chemistry – A European Journal* **21**, 16601–16608 (2015)], © 2015 WILEY-VCH Verlag GmbH & Co. KGaA, Weinheim.

The disadvantages of VDP analysis are, similar to BV methods discussed in the next section, that no dynamic process can be analysed directly, since VDP deals only with static crystal structures. A second disadvantage is that the VDP analysis is based on the assumption of completely ionic bonds. This may be a permissible simplification for oxygen-containing materials, due to the high electronegativity of O. Less-electronegative elements are, however, more easily polarisable, forming bonds of a higher covalency that tend to shield charges. Due to the geometrical fundamant of this methodology, very complex conduction patterns may be generated, especially in low-symmetry compounds that are difficult to interpret. The same holds for large intra-structural voids that the algorithm may tessellate into a multitude of vertices very close to each other. Some algorithms have been added to the programme in the recent years to allow, for instance, void-merging and the calculation of VDP in the channels between voids. Generally speaking, even though the geometry can be seen as an expression of the energetic relations in the crystal structure, energetic calculations offer a deeper understanding than sole geometry. For instance, since there is a preferential bond length between atoms (depending on the chemical surrounding), a void becomes less favourable if it is too large or too small. The most important feature of a good ion-diffusing material is its low-deviation energetic landscape for the pathway of the diffusing ion. This energetic landscape is not directly accessible by evaluating geometrical volume sizes in crystals. Further developments of the VDP methodology could therefore comprise the calculation of energetic parameters and an optimisation towards the applicability on the cation-conduction at hand.

2.3 Example 1: Li-ion conductors

In a first work, it was shown that the VDP method is an excellent tool to analyse crystalline solid electrolytes [70]. It reveals the ionic conduction channels of well-known cationic conductors, their dimensionalities, and allows a differentiation between so-called significant and probabilistic voids and channels. The latter may describe channels that could be activated at higher energies (temperatures). These works were expanded by screening the ICSD for compounds containing at least both Li and O and analysing all void-networks for their possible Li-ion conduction [14]. These materials were both ternary and quaternary compounds with the third and fourth element being any other chemical element. Furthermore, compounds with disorder on the O-sites were excluded yielding databases for ternary and quaternary structures with 822 and 1,349 entries, respectively. All voids' and channels' sites and sizes within were identified and evaluated according to the principles introduced above. The topologies of these networks were furthermore analysed with ToposPro.

Within the results, a total of 26 compounds have been predicted as suitable Li-ion conductors, while 126 structure types were found, already described in the literature as solid electrolytes (Table 1).

Table 1: Substances with possible Li-ion conductivity and their ICSD collection code [14]. “Dim” stands for dimensionality of the conduction network.

Formula	ICSD-#	Dim	Formula	ICSD-#	Dim	Formula	ICSD-#	Dim
Li_3AuO_3	15113	1D	$\text{Li}_{0.33}\text{MoO}_3$	201959	1D	Li_4TeO_5	2403	1D
$\text{Li}_2\text{Al}_2\text{Si}_4\text{O}_{12}$	98845	2D	$\text{Li}_2\text{Mo}_4\text{O}_{13}$ (HT)	4155	1D	$\alpha\text{-Li}_2\text{Te}_2\text{O}_5$	26451	1D
Li_3BiO_3	85072	1D	$\text{Li}_2\text{Mo}_4\text{O}_{13}$ (LT)	6134	3D	$\beta\text{-Li}_2\text{Te}_2\text{O}_5$	26452	1D
Li_5BiO_5	203031	1D	$\text{Li}_4\text{Mo}_5\text{O}_{17}$	85439	1D	Li_2UO_4 (<i>Pnma</i>)	200297	1D
LiBUO_5	67114	1D	LiReO_4	37118	1D	Li_2UO_4 (<i>Fmmm</i>)	20508	3D
Li_3CuO_3	4201	1D	Li_5SbO_5	203030	1D	Li_4UO_5	20452	1D
$\text{Li}_3\text{CuSbO}_5$	51392	1D	$\text{Li}_{10}\text{Si}_2\text{PbO}_{10}$	78326	3D	Li_6UO_6	48209	3D
$\text{Li}_3\text{Er}(\text{NO}_3)_5(\text{NO}_3)$	401554	1D	Li_2TeO_3	4317	1D	$\text{Li}_{0.88}\text{U}_3\text{O}_8$	69846	2D
$\text{LiFe}(\text{SeO}_3)_2$	75554	3D	Li_2TeO_4	1485	3D			

2.4 Example 2: Na-ion conductors

For the long-term, large-scale energy storage in the 100 MW range the Na-S battery technology accounts for the largest market share [72, 73]. A Na-S battery, invented in the 1960s [74], was enabled by the discovery of β -alumina, which shows a high conductivity for Na-ions at the operating temperature of 300 °C [75]. This material works as separator as well as solid electrolyte in the Na-S battery. Due to the high operation temperatures of high-temperature Na-S batteries and the intense reaction between Na and S at these temperatures, only ceramic, glass-ceramic, or glass electrolytes can be used [76–78]. New solid electrolyte materials are necessary for decreasing the operation temperature and thus to increase energy density and safety.

In Refs. [27] and [19], it was shown that VDP analysis is a suitable and highly promising approach for the identification of novel (Na^+) ion conducting materials. It was firstly shown that by using the Voronoi-Dirichlet approach, well-known Na-ion conductors could be clearly identified and, moreover, new promising candidates have been determined.

A data mining was first carried out to find the most recurring geometrical values within compounds containing at least Na and O. As described in Ref. [65], VDP analysis works only for same-anion-neighbourhoods due to the problem of the division coefficient. Hence, we decided to search within O-containing compounds, since the best-known Na-ion conductors are oxides. All compounds comprising at least these two chemical elements were filtered from the ICSD 16/1 first [79]: 11,004 out of 183,804 entries. After all duplicates⁶ were deleted (9,152 remaining), all compounds whose chemical formula did not match the composition of the atomic positions⁷ were deleted as well, resulting in 5,541 compounds. In Figure 6, the general handling and processing routine of the data up to the results is visualised. For the data mining, only well-defined structures without any disorder are used, to avoid geometry and bond length changes due to, e.g., Vegard’s law. Within this data, all VDP for every site in the structure are constructed and all Na atoms only coordinated by O are taken into account. Mean values for r_{SD} , G_3 , $R_{\text{Na}-\text{O}}$, and maximum solid angles for weak Na-to-metal contacts were considered. In Figure 7, two plots and their discussion are presented.

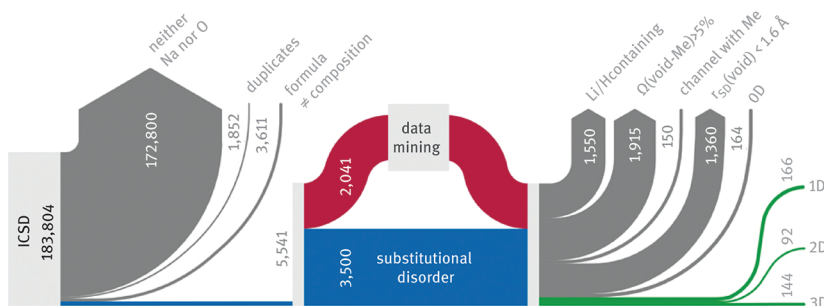


Figure 6: Graphical representation of the typical data handling and processing as well as obtained promising candidates for Na-ion solid electrolytes. Scheme was adapted from [27].

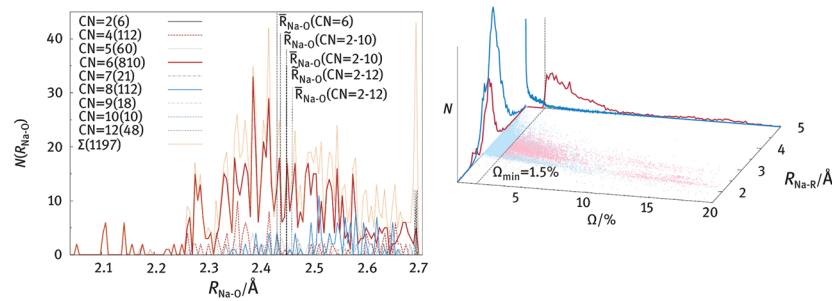


Figure 7: Left: Depiction of the distribution of naturally occurring interatomic distances of Na–O as taken from [27]. Different mean values (given in $\langle \dots \rangle$) and medians (“M”) are presented. Some coordination numbers are chemically meaningless but due to the algorithms of ToposPro, some distances to O may be interpreted already as weaker bonds and not counted to the coordination number (or inversely). Right: 3D representation of the solid angles and interatomic distances of Na-to-non-O atoms. The blue graphs represent data points of nearest neighbours, whereas the red colour indicates post-next-neighbours showing distinct regions. Therefore, a clear border between nearest neighbours (strong bonds) and post-nearest neighbours (weak bonds) can be drawn. This data was accumulated during the work done for Ref. [27].

These values were used to analyse the three best-known and technologically already used Na-ion conductors β -alumina, NaSICON, and Na rare-earth silicates (Figure 8). VDP can describe the conduction mechanism with regard to path-dimensionality and the Na- and void sites incorporated in the conduction process. Furthermore, the void-descriptors (r_{SD} -magnitudes and Ω of non-O contacts) show striking similarities between these compounds, allowing the deduction of prerequisites for the VDP method applied to crystalline O-containing Na^+ -conductors. Compared to the data-mined r_{SD} values ((1.523 ± 0.040) Å), higher numbers (1.6 Å) are observed for the migration paths and very low deviations between inequivalent sites. None of the voids are constituted by (next-) neighbour metal ions with solid angles larger than 5 % and all channels are constituted by oxide-ions. Because of the strong correlation, these findings are applied to the database of compounds containing at least Na and O to find materials with similar features to the established ion conductors.

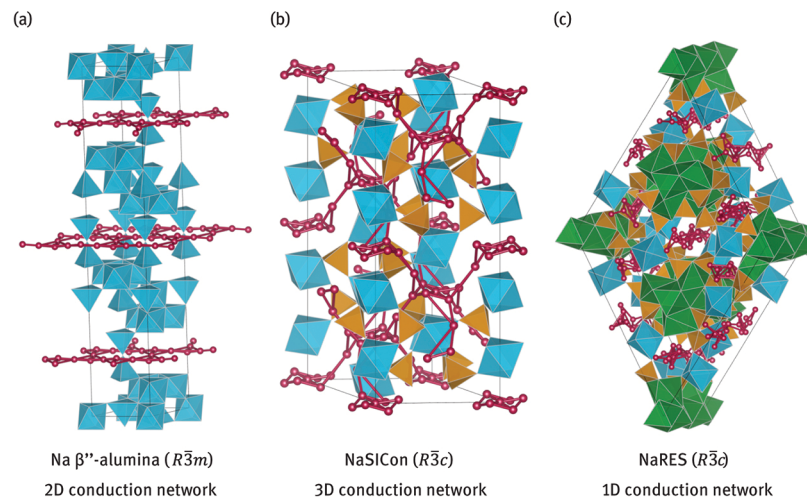


Figure 8: Crystal structure and conduction network of the well-known Na-ion conductors. Blue polyhedra: MO_x polyhedra, orange polyhedra: TO_4 -tetrahedra, green polyhedra: NaO_x polyhedra, red dots and segments: voids and channels of the conduction network as determined with VDP. Subfigure (a): $M = \text{Al}$; (b) $M = \text{Zr}$, $T = \text{Si}, \text{P}$; (c) $M = \text{RE}$ (e.g. Y), $T = \text{Si}$. In the right-most case, also a 3D conduction is observable if slightly smaller voids are considered [19]. Best achieved room temperature conductivities for these materials range up to a maximum of 10^{-3} to 10^{-1} S/cm [80–82].

Eventually, the VDP for all compounds (now again including disordered compounds) are constructed. During this step, all Na positions need to be neglected. All VDP vertices indicate structure-immanent void spaces in the structure with some of those corresponding to Na positions in the structure. In order to find the migration maps, the two factors “determination” and “comparison” mentioned above have to be checked. Therefore, all voids with void-metal solid angles larger than 5 %, as well as channels constituted by metal atoms are excluded (determination). Eventually, the same procedure is carried out for voids with $r_{SD} < 1.6$ Å (comparison). Those voids and channels still remaining and percolating through the structure are geometrically similar to those conduction systems found in the best-known solid Na-conductors. The final step is the analysis of the dimensionality of the identified conduction networks into 0D (non-percolating loops), 1D, 2D, and 3D systems. The whole algorithm is graphically demonstrated in Figure 5 and Figure 6, whereas the latter is showing a so-called

Sankey diagram with the typical data flow during the whole VDP approach. Figure 9 further shows a possible systematisation of the results as taken from Ref. [27].

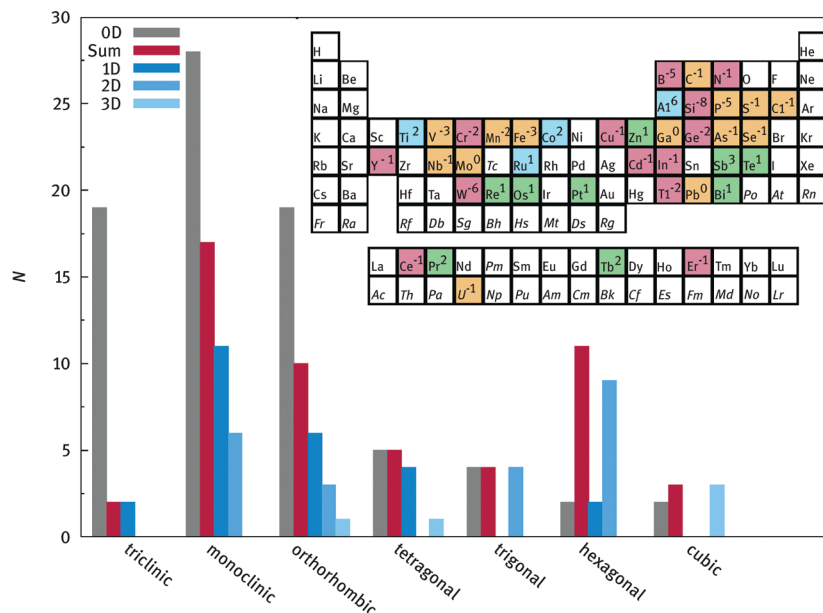


Figure 9: Systematisation of the results of Ref. [27], according to the crystal systems observed in the identified compounds. Mainly, non-percolating compounds are found to have lower-symmetry crystal classes, while, the higher the dimensionality of the conduction network, the higher the symmetry of the compound. The inset shows the elements mainly observed accompanying Na and O in the ternary Na oxides. The colour green symbolises elements that were only found in compounds with only non-0D conduction networks, blue decodes compounds with mainly non-0D, orange mainly 0D and red only 0D conduction networks. The number describes the amount of compounds observed with this element; compounds that show only 0D migration maps are counted as negative.

The data collected from the analysis allowed a screening of 402 materials out of the ICSD. Not only well-known conductors but also new potential solid Na electrolytes are identified. Due to the high number, a further differentiation is necessary, since, according to the Voronoi-Dirichlet approach, all compounds should be highly promising. A rating system is introduced containing a total of eight crystallographic and economic parameters in order to find those materials with the highest promise for a further electrochemical analysis. Regarding these parameters, the chapters “Fundamental principles of battery design” and “Separators and solid electrolytes” of Ref. [50] will explain the crystallographic/energetic parameters more in-depth: The best compounds should have low standard deviations of the void-sizes, high dimensionalities of both matrix and conduction network, a high-symmetry crystal class, and a low amount of non-equivalent void sites with high-multiplicity and low occupancy. From the economic point-of-view, the criticalities [83] of the constituting elements can be considered and a virtual price can be calculated. Lastly, the density can be taken into account. Low values for any of these three should be preferential. In Table 2, the most promising candidates according to this methodology are summarised. For a more in-depth view on these materials, Ref. [19]’s table is recommended.

Table 2: Most promising candidates for Na-ion conductors as identified by VDP.

Formula	ICSD-#	Notes
$\text{Na}_8(\text{AlSiO}_4)_6(\text{NO}_3)_2$	413038	Unstable, single O ion in the structure
$\text{NaAl}(\text{SiO}_4)$	34884	Determined at 750 °C
$\text{Na}_2(\text{Al}_2\text{Si}_3\text{O}_{10})$	83013	Determined at 550 °C; shows void clusters
$\text{Na}(\text{AlSiO}_4)$	85553	
$\text{Na}_2\text{FeTi}(\text{PO}_4)_3$	92226	Described as Na-ion conductor
$\text{Na}_2(\text{Al}_2\text{Si}_3\text{O}_{10})$	157309	Theoretical structure
NaOs_2O_6	246504	Theoretical structure
$\text{Na}_{3.70}\text{Ca}_{1.15}\text{Ge}_3\text{O}_9$	65017	
$\text{Na}_{1.72}(\text{Cr}_{1.71}\text{Ti}_{6.29})\text{O}_{16}$	79502	Described as Na-ion conductor
$\text{Na}_{7.85}\text{Al}_{7.85}\text{Si}_{8.15}\text{O}_{32}$	108334	Determined at 100 °C
$\text{Na}_{7.85}\text{Al}_{7.85}\text{Si}_{8.15}\text{O}_{32}$	108387	Determined at 600 °C
$\text{Na}_{2.62}\text{V}_2(\text{PO}_4)_2(\text{O}_{1.6}\text{F}_{1.4})$	191947	Described as Na insertion compound

Na ₅ (MnO ₄)	47101	
Na ₂ (Al ₂ Si ₃ O ₁₀)	160820	Determined at 500 °C
Na ₂ TiOSi ₄ O ₁₀	16899	
Na ₂ Mg ₃ Zn ₂ (Si ₁₂ O ₃₀)	77121	
Na _{1.92} (Al ₂ Si ₃ O ₁₀)	83012	Determined at 300 °C
Na _{1.78} (Mg _{1.87} Al _{0.13})(Si ₂ O ₇)	92968	High-pressure synthesis

Due to its simple algorithm, the methodology can be easily applied to large structural databases to calculate all important data in a very short time even on desktop and laptop computers without the use of large CPU power. It is therefore a very fast, high-throughput data mining routine. As already mentioned, a disadvantage of the methodology is that it is only applied to static crystal structures and that no direct energetic evaluation is possible. This could be subsequently done using bond valence (BV) site-energy calculations (see Section 3) or density functional theory (see Section 4) computations.

3 Bond valence methods

3.1 Introduction

BV based methods are capable of calculating potential ion pathways, intercalation sites, and giving a rough estimation of the activation energy of ion conduction for one structure within a few minutes or hours. Therefore, BV approaches represent a valuable tool to pick out potential targets among thousands of structures. The history and fundamentals as well as all modern applications are comprehensively described in the textbook by Brown and Poeppelmeier [84].

The foundation of the BV theory has been already laid in the 20s of the last century by Pauling's heuristic electrostatic valence principles, especially the principle of local charge neutrality [85]. As an early estimate of what we call the *bond valence* today, he defined the bond strength as the valence of the cation divided by the number of bonds it forms with its counterions, which equals the number of nearest anionic neighbours. The valence equals the number of electrons (/electron holes in the valence shell) used in bonding and is positive (/negative) for cations (/anions). It is thus used to calculate the stoichiometry of compounds and is often equated with its oxidation state [86]. This principle, however, is far from giving quantitative results, since the deviation of the sum of the Pauling bond strengths to the actual valence of ions accounts for up to 40 % [84]. Only almost four decades later, in the 1960s, with the advent of sufficiently accurate experimental techniques for structure determination, it was possible to illuminate how the bond length correlates with properties like the coordination number and the formal oxidation states. For instance, it was found that the bond length between the same ionic pairs depends on the coordination number, being larger when the coordination number is higher. Additionally, Baur recognised that there is a quantitative correlation between the deviation of the Pauling bond strength (over- or underbonding) and the bond length [87]. Finally, in 1970, Donnay and Allmann [88] introduced the term *bond valence* in order to describe the bond strength. They proposed a power law with fitted constants for each coordination sphere to calculate experimental BVSs from known bond lengths. By this means, they were able to locate missing hydrogen atoms during structure determination. Today, an exponential term that was published in 1985 by Brown and Altermatt [89] together with an extensive list of fitted BV parameters is utilised to calculate BVs:

$$BV = \exp \left\{ \frac{R_0 - d}{b} \right\}, \quad (1)$$

with R_0 and b as empirical BV parameters for a specific pair of atoms, and the distance d between two actual atoms. The empirical constants are accessed by analysing thousands of known crystal structures. They are fitted in a way that for a BV of a considered ion the sum of all BVs with its counter ions (BVS) equals its valence in the equilibrium state. Conversely, if the BVS for the considered ion is calculated for positions in the lattice of examined compounds, the mismatch between the BVS and formal oxidation state of the considered ion shows accessible sites: The smaller the bond valence sum mismatch (BVSM), the more favourable is this position for the ion. A stable site may show a deviation of less than 10 % [90]. Therefore, the BVS approach is still widely applied in crystal structure verification and locating of very light elements (which would be otherwise only hardly accessible) in crystal structure determination in the case of predominantly ionic and covalent compounds.

Despite of this success of the BV theory, a theoretical base of the concept of the chemical bond was only derived in the late 90s by Preiser *et al.* [91]. He showed that in unstrained structures the BV correlates well with the bond flux, which is the electrostatic flux that links neighbouring ions of opposite charge. It is calculated by

replacing the ions at their determined positions by point charges and is shown exemplary for the Ca–O bond in Figure 10. Corroborated by the quantitative agreement with experiment and the secure theoretical foundation, the BV theory found many applications in analysing, modelling, and also predicting complex atomic structures in crystals, glasses, and even liquids and helps to understand its resulting physical properties.

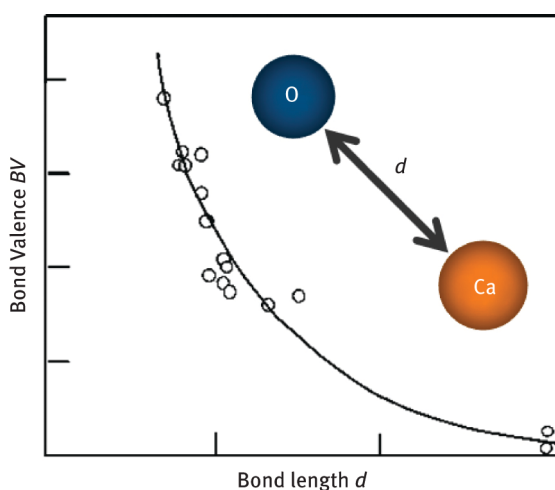


Figure 10: Bond valence–bond length correlation for observed Ca–O bonds adapted from [92] with data from Ref. [91] reproduced with permission of the International Union of Crystallography. The line calculated from Eq. 1 corresponds well with the circles that represent calculated bond fluxes for a number of experimentally determined bond lengths (*Crystallography Journals Online*; <https://journals.iucr.org/>).

3.2 BV approaches for analysing compounds with fast ionic transport

Besides the main applications of assessing the plausibility of crystal structure models and of locating light elements in crystal structures, the BV methodology has been applied for the analysis and prediction of ionic conductors and intercalation compounds: Corresponding to the resolution, BVSM values are calculated for every voxel in the three-dimensional unit cell of the examined compound. As mentioned before, in general low deviations of the BVS and formal oxidation state of less than 10 % are thought to indicate available positions for the considered ion [90]. If these positions percolate, i.e. form a continuous path through the unit cell, ionic conduction is assumed to be possible. In 1982, the applicability of the BVSM method for ion conductors was demonstrated for the first time by examining the Ag^+ ion conductors $\alpha\text{-AgI}$ and $\text{Ag}_{16}\text{I}_{12}\text{P}_2\text{O}_7$ [93]. A close agreement of plots with small BVSM for Ag^+ with experimentally derived atomic displacement parameters was shown, demonstrating the capability to predict migration pathway topologies and to identify the sites involved in ion conduction. Besides the comparison with atomic displacement parameters, ion distribution maps derived by the maximum entropy method as well as MD and DFT approaches suggest the applicability of the BVSM analysis to find ionic pathways of Ag^+ [34], Na^+ [39], Li^+ [16], Cu^+ [39], F^- [90], and O^{2-} [39, 90], and even WO_4^{2-} [90, 94] in crystalline materials, which is shown exemplary in Figure 11. Consequentially, BV analysis has been widely used for the analysis [34, 39, 95–101] and screening [16, 17] of solid electrolytes and intercalation electrodes for monovalent ions. Given some examples of fast ionic transport pathways for O^{2-} [39, 95], a thorough screening for solid conductors for fuel cells could be fruitful as well, yet it has not been performed up to now. Concerning amorphous materials, the BV approaches can be applied as well, provided a local structure model is generated first. This has been obtained by MD or reverse MC modelling of experimental data [42–45].

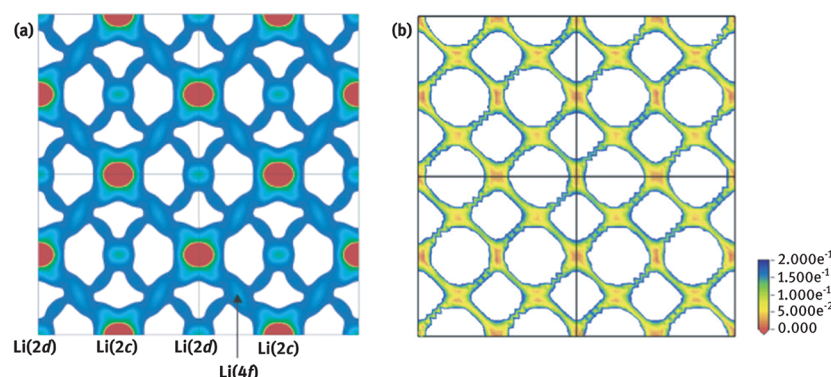


Figure 11: Comparison of experimentally determined ion migration paths with BVS maps for $\text{Li}_{0.62}\text{La}_{0.16}\text{TiO}_3$ on the (002) plane: (a) Li-ion distribution derived by the analysis of neutron diffraction data reconstructed by the Maximum Entropy Method (Reprinted with permission from [178]. Copyright 2005 American Chemical Society) and (b) BVSM data (Reprinted from [16], Copyright 2012, with permission from Elsevier).

An extensive collection and analysis of BV methods for understanding ionic conduction can be found in Ref. [38]. Especially Adams and his co-workers established and improved the methods by introducing softBV parameters which consider also post-first-coordination-shell atoms [102]. A detailed discussion on the bias introduced by neglecting interactions with counterions from higher coordination shells and on the role of the bond softness parameter b in equation 1 can be found in [103]. Essentially, the choice of a realistic value of b for a given cation-anion pair enhances the link between BVSM and site energy and particularly enhances the predictions for mobile cations in environments with different types of immobile cations.

One reason for occurring differences of BVSM results to experiment or DFT predictions has been assigned to the hard-sphere exclusion approach previously applied for treating interactions between immobile and mobile cations [38]. This issue is implicitly closely related to the use of fixed threshold values in the elimination of cation-neighboured polyhedra from the VDP pathway models. The method has been developed further to take Coulomb repulsions into account and thereby to eliminate the need for such hard-sphere exclusion radii. From the first BVSM models it was explored, whether BVSM results can be utilised to directly predict experimentally observable properties of ionic conductors. This first led to the establishment of a close correlation between the volume fraction of regions with a sufficiently low BVS mismatch and the activation energy of Ag^+ ion conducting glasses [42, 104]. Since for the highly disordered ion conducting glasses the prefactor of the Arrhenius equation hardly varies this also implied a correlation between the pathway volume fraction and the ionic conductivity. A mass scaling compensating for the ion mass dependence of the attempt frequency of the mobile ion even allows to derive a common master curve for these pathway volume fraction relationships in alkali and silver ion conducting glasses [43] and helped to quantitatively describe the mixed mobile ion effects in various such glasses [105, 106]. A direct link to the energy has finally been worked out in 2009 [37], which is illuminated in the following section.

3.3 The bond valence site energy method

The BVSE method [37, 107], which is also referred to as BV energy-landscape analysis, is designed to roughly estimate the migration barrier in ion conductors from a static structure model. For this purpose it attempts to calculate the energetic environment of mobile ions by translating the BV into a bond energy value by means of a Morse-type potential. The Morse-type interactions between cations and anions in the BVSE potential are complemented by terms for the screened Coulomb repulsions among cations as well as among anions. In general, a broad agreement with both experimental data and other modelling techniques such as DFT and MD can be observed for the migration paths and the subset of the atomic sites taking part in the conduction for the mentioned monovalent ion species [18, 39, 107–109] (Figure 12).

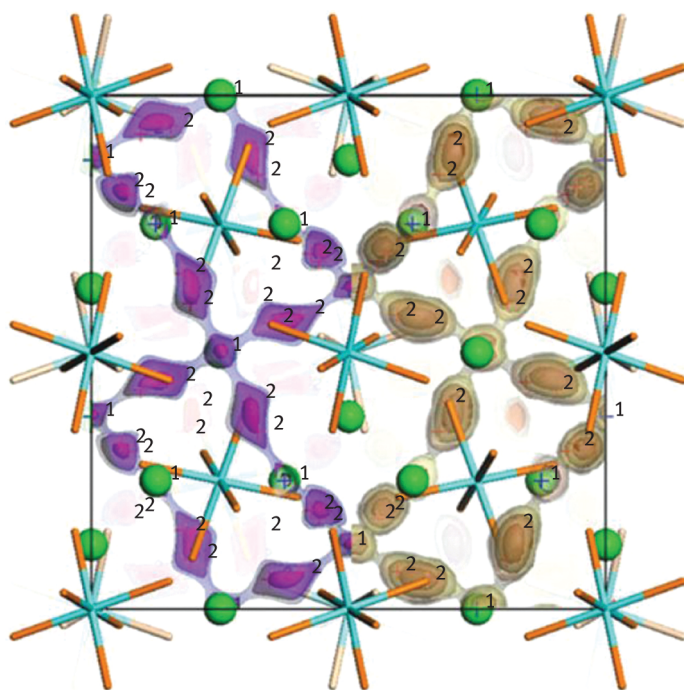


Figure 12: Li^+ pathways in $\text{Li}_7\text{La}_3\text{Zr}_2\text{O}_{12}$ determined for the cubic high-temperature phase by BVSE (left-hand side) and MD (right-hand side). The pathways in the rear part of the unit cell are shown in pale colours for better distinction and the numbers assign the different Li sites. Reprinted with permission of Springer from [38].

In comparison to VDP analysis, the prediction of complex curved paths is possible [107]. On the other hand, as in the Voronoi-Dirichlet approach, the relaxation of the surrounding atoms as well as electronic structure during migration cannot be directly taken into account, since the BVSE is calculated for a static structure. As relaxation would release local stress and may thus lower the total energy, the BVSE migration barrier is generally thought to be higher than the experimental value [38]. While the overestimation in framework structures can be easily factored in by scaling the predicted migration barrier, typically by a factor 0.8. Layered structures that are held together by weaker interlayer forces would show a more pronounced relaxation by widening of the interlayer spacing so that a reduced scaling factor of only 0.4 may be appropriate, e.g. for the Li^+ transport in layered transition metal oxides Li_xMO_2 [38]. Nevertheless, for monovalent ions there is enough data to compare to and it appears there is a good correlation between experimental and BVSE activation energies. An extensive study, which gives an exact formula for the correlation, is still waiting to be published soon. However, the recent work of Xiao *et al.* [18] as well as Nishihitani *et al.* [110] already demonstrates the strong correlation of BVSE and DFT barriers, which is a suitable comparison, as experimental data could also contain contributions from grain boundaries.

Some programmes are specially designed to calculate BVSM/BVSE over three-dimensional grids (e.g. Bond_Str within the FULLPROF suite, Juan Rodríguez-Carvajal (2010)) and also find their thresholds for ion migration through the structure (3DBVSMapper [39]). It may be cautioned that the original version of 3DBVSMapper overestimates migration barriers. However, since these programmes do not permit the automatic calculations for abundant structures in batch mode, most authors fall back on self-programmed scripts for their screenings [35, 36, 110]. A beta version of a new softBV code suitable for screening ordered structures is available from the authors [111].

To exemplarily demonstrate the information that can be extracted by this method, BVSE models are calculated for all materials identified by the VDP approach of the previous section (Table 3). Additional details of the pathways can be extracted in this way, as shown in Figure 13. Firstly the BV analysis yields a qualification of the plausibility of the crystal structures. By chance, the collection contains one example, $\text{Na}_8(\text{AlSiO}_4)_6(\text{NO}_3)_2$, for which the literature structure refinement in ICSD-# 413038 is obviously wrong leading to a high global instability index (GII), while exchanging the assignment of the Al and Si site leads to a much more plausible structure model. The GII is defined as the root mean square mismatch of the BVS. For the plausible structure models, the BVSE approach predicts migration barriers ranging from $E_{\text{mig}} = 0.05 \text{ eV}$ up to 0.7 eV . Hence, based on the migration energy, these compounds potentially show technologically interesting room temperature conductivities of 10^{-3} S/cm , while for others the BVSE method suggests that the conductivity is too low to be of practical usefulness. The example $\text{Na}_{3.70}\text{Ca}_{1.15}\text{Ge}_3\text{O}_9$ (ICSD-# 65017) with a mixed $\text{Na}^+/\text{Ca}^{2+}$ occupancy is seen to be a moderate Na^+ ionic conductor only when analysing a local structure model. Here, this was done by automatically generating a $P1$ supercell wherein Na and Ca are randomly distributed on the sites that are symmetry

equivalent in the average structure. Still, these predictions will be somewhat less reliable, unless the supercell is subjected to a relaxation. For the hollandite-type structure $\text{Na}_{1.72}(\text{Cr}_{1.71}\text{Ti}_{6.29})\text{O}_{16}$ the low migration barrier in the strictly 1D channels will not translate into a fast ionic conductivity in bulk materials, as such strictly 1D conductors are easily blocked by point defects. In contrast, the related quasi-1D conductors $\text{Na}_{7.85}\text{Al}_{7.85}\text{Si}_{8.15}\text{O}_{32}$ and $\text{Na}_{7.85}\text{Al}_{7.85}\text{Si}_{8.15}\text{O}_{32}$ may be expected to show interesting ionic conductivity as the fast ion-conducting channels are interconnected with an only moderately higher energy barrier.

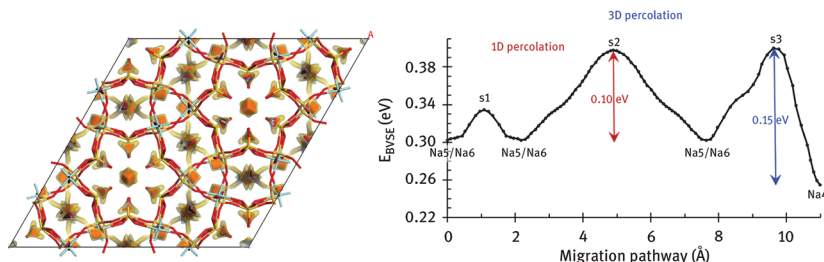


Figure 13: BVSE model of Na^+ migration pathways in $\text{Na}_5\text{YSi}_4\text{O}_{12}$ from the crystal structure model in ICSD-# 20271 shown as isosurfaces of constant BVSE projected on the a - b plane (left-hand side) and as energy-landscape diagram (right-hand side). Here, Na^+ BVSE are specified relative to the energy of the lowest-energy Na site, the immobile $\text{Na}3$. The pathways of lowest migration barrier ≈ 0.10 eV among the partially occupied $\text{Na}5/\text{Na}6$ sites are predicted to be the same channels along c -direction identified by VDP (shown in orange). While such 1D channels alone would be highly vulnerable to blocking by point defects, the BVSE model shows that they are interconnected by perpendicular pathways $\text{Na}5/\text{Na}6$ to $\text{Na}4$ with an only slightly higher migration barrier of 0.15 eV explaining the experimentally observed fast ionic conductivity.

Table 3: Predictions from BVSE analysis of the same crystal structures discussed above in the section on the VDP method. For ordered stable phases a value of the GII > 0.2 is normally taken as an indication that there is something wrong in the crystal structure determination. For plausible structures the migration energy E_{mig} and the pathway dimensionality d_{path} as well as a rough range of expected room temperature ionic conductivities σ_{RT} for this structure are suggested. For undoped materials, where defect formation energies have to be considered, the order of magnitude of the Na^+ ion conductivity is expected to be near the lower end of this range or even much lower, while a suitable doping might push the conductivity of this structure type up to the upper limit of this range. For more information on the calculation of the conductivities we refer to Ref. [111].

Formula	ICSD-#	GII	E_{mig} (eV)	d_{path}	Expected $\log(\sigma_{\text{RT}}/\text{S}$ $\text{cm}^{-1})$	Notes	Lit.
Na β-alumina	74473	0.135	0.046	2D	-2.0 to -2.3	$\exp. \log(\sigma_{\text{RT}}) \approx -2.6$	[112]
NaSiCon (high):							
$\text{Na}_{3.05}\text{Zr}_2\text{Si}_{2.05}\text{P}_{0.95}\text{O}_{12}$	62383	0.176	0.175	3D	-2.7 to -3.5	$\exp. \log(\sigma_{\text{RT}}/\text{S cm}^{-1}) = -3.1$	[113]
$\text{Na}_3\text{Sc}_2(\text{PO}_4)_3$	65407	0.059	0.293	3D	-3.6 to -5.0	$\exp. \log(\sigma_{\text{RT}}/\text{S cm}^{-1}) = -4.6$ (by extrapolation)	[114]
$\text{Na}_3\text{Sc}_2(\text{PO}_4)_3$	84036	0.075	0.231	3D	-3.1 to -4.2	$\exp. \log(\sigma_{\text{RT}}/\text{S cm}^{-1}) = -4.6$ (by extrapolation)	[115]
$\text{Na}_3\text{MgZr}(\text{PO}_4)_3$	172806	0.048	0.295	3D	-3.6 to -5.0	$\exp. \log(\sigma_{\text{RT}}/\text{S cm}^{-1}) = -5.2$	[116]
$\text{Na}_3\text{MgNi}(\text{PO}_4)_3$	172807	0.048	0.338	3D	-3.9 to -5.6		[116]
$\text{Na}_3\text{V}_2(\text{PO}_4)_3$	248140	0.071	0.369	3D	-4.2 to -6.1		[117]
$\text{Na}_5\text{YSi}_4\text{O}_{12}$	20271	0.101	0.095	1D	-2.5 to -3.2	$\exp. \log(\sigma_{\text{RT}} = -2.95)$	[118]
$\text{Na}_8(\text{AlSiO}_4)_6(\text{NO}_3)_2$	413038 ^a	0.455	0.619	3D	-	Wrong assignment of Al/Si in lit. refinement?	[119]
$\text{NaAl}(\text{SiO}_4)$	0.145	0.656	3D	-7 to -10.8	After exchanging Al and Si sites	[120]	
Na₂(Al₂Si₃O₁₀)	83013	0.133	0.217	3D	-3.8 to -5.4^b	High-temperature phase determined at 750 °C	[121]
$\text{Na}(\text{AlSiO}_4)$	85553	0.056	0.639	3D	-3.0 to -4.0 ^b	Natrolite high, dehydrated; determined at 550 °C	[122]
$\text{Na}_2\text{FeTi}(\text{PO}_4)_3$	92226	0.198	0.594	3D	-6.8 to -10.5		[123]
$\text{Na}_2(\text{Al}_2\text{Si}_3\text{O}_{10})$	157309	0.132	0.514	3D	-6.4 to -9.7	Described as Na-ion conductor; exp. $\log(\sigma_{\text{RT}}/\text{S cm}^{-1}) \approx -8$	[124]
NaOs_2O_6	246504	0.2 ^c	0.191	3D	-5.6 to -8.3	Theoretical structure	[125]
$\text{Na}_{3.70}\text{Ca}_{1.15}\text{Ge}_3\text{O}_9$	65017	0.155	0.324	supercell	-2.8 to -3.7	Theoretical structure; Na position questionable, non-integer oxidation state for Os → mixed conductor	[126]
$\text{Na}_{1.72}(\text{Cr}_{1.71}\text{Ti}_{6.29})\text{O}_{16}$	79502	0.091	0.051	1D	-3.8 to -5.4	Na/Ca disorder on same site; BVSE analysis based on supercell	[127]
$\text{Na}_{7.85}\text{Al}_{7.85}\text{Si}_{8.15}\text{O}_{32}$	108334	0.096	0.051	1D	Superionic ^d	Proposed as Na ⁺ ion conductor, but no conductivity data. As for other hollandite-type structures the high, strictly 1D Na ⁺ ion mobility can only be utilised in nanocrystals.	[128]
$\text{Na}_{7.85}\text{Al}_{7.85}\text{Si}_{8.15}\text{O}_{32}$	108387	0.186	0.678	3D	Superionic ^d	Determined at 100 °C; average structure	[128]
$\text{Na}_{2.62}\text{V}_2(\text{PO}_4)_2(\text{O}_{1.6}\text{F}_{1.4})$	191947	0.781	(0.461)	3D	-	Structure model wrong (very high GII); described as Na insertion compound	[129]
$\text{Na}_5(\text{MnO}_4)$	47101	0.304	0.188	3D	(-2.8 to -3.7)	High GII , all BV sums low. (early Rietveld powder structure)	[130]
$\text{Na}_2(\text{Al}_2\text{Si}_3\text{O}_{10})$	160820	0.138	0.527	3D	-5.7 to -8.5 ^b	Determined at 500 °C	[131]
$\text{Na}_2\text{TiOSi}_4\text{O}_{10}$	16899	0.133	0.577	3D	-6.2 to -9.4		[132]

$\text{Na}_2\text{Mg}_3\text{Zn}_2(\text{Si}_{12}\text{O}_{30})$	77121	0.151	0.286	2D	-3.5 to -4.9	[133]
$\text{Na}_{1.92}(\text{Al}_2\text{Si}_3\text{O}_{10})$	83012	0.136	0.489	3D	-5.3 to -7.9 ^b	[120]
$\text{Na}_{1.78}(\text{Mg}_{1.87}\text{Al}_{0.13})(\text{Si}_2\text{O}_7)$	92968	0.171	0.263	2D	-3.3 to -4.6 ^c	[121]

^a Bond valence sum test shows that Al and Si have been mixed up in this structure refinement. After exchanging the sites the GII drops to the plausible range. However, this stable structure is found to be not a good conductor.

^b If this high-temperature phase can be retained at room temperature.

^c With BV parameters for Os^{6+} instead of $\text{Os}^{5.5+}$.

^d To be ascertained by a local structure model.

4 Density functional modelling and the materials project

4.1 Introduction

The methods VDP and BVSE presented in the preceding sections to assess battery materials are based on the analysis of static crystal structures. However, ionic movement in a crystal is in general an interconnected dynamic process of atomic as well as electronic movement up to the collective migration of whole atomic units. Thus, the static energy barrier approximation of BVSE can be a rough estimation, only. Compared to other *ab initio* methods, DFT offers a fast quantum mechanical methodology to include the relaxational degrees of freedom and to model any crystalline material *ab initio* providing next to the migration barriers also the full electronic structure and an access to electronic conductivity parameters.

The electronic structure determines most material properties of a crystal. Electrons are of quantum nature and in the quantum-dynamical picture, according to Heisenberg's uncertainty relation, position and momentum of an electron can be simultaneously determined only up to a limit $\Delta x \cdot \Delta p \geq \hbar/2$. In an eigenstate of certain quantum numbers, its position in space can therefore be described with a probability density. Quantum particles, even if they have a mass, show interference with each other like waves. They are indistinguishable from another. This realisation is the foundation of DFT.

The general equation that describes a quantum mechanical system of electrons and nuclei in the non-relativistic case is the Schrödinger equation. In its stationary form with no explicit time dependence on the potential, it represents the energy relation as an eigenwert equation with energies E_i for the respective Hamiltonian \hat{H} . With the many-body wavefunctions $|\Psi_i\rangle \leftrightarrow \Psi_i(x_1, x_2, \dots, x_N, R_1, R_2, \dots, R_M)$ in dependence of $3(N + M)$ spatial coordinates x and R of the N electrons and M nuclei and N electronic spin states ($x = \{r, s\}$) as solutions it reads $\hat{H}|\Psi_i\rangle = E_i|\Psi_i\rangle$. Since the nuclei are several orders of magnitude heavier than the electrons, the Born-Oppenheimer approximation can be applied, solving the electronic terms in the potential of fixed nuclei positions (for details see e.g. [134]). Still, it requires immense computational efforts to take into account all distinct electron position vectors x_1 , as is done e.g. in Hartree-Fock calculations, and only systems very limited in size can be modelled.

This limitation is overcome by the idea of a general electron density, as has been already used in the Thomas-Fermi model [135, 136] (1927) treating all electrons as a uniform electron gas or later by Slater [137] (1951) giving a local density expression for the Fermi hole and thus simplifying the non-local Hartree-Fock exchange. But the revolution of atomistic structure calculations on the quantum level took place only after the theorems of Hohenberg and Kohn [138] (1964), which prove that "the full many-particle ground state is a unique functional of $\rho(r)$ " and that only the true ground state density $\rho(r)$ yields the lowest total energy. These proofs gave rise to base quantum calculations on the presumption of the ground state electron density, which uniquely determines the system, the Hamiltonian as well as all other physical and chemical properties (e.g. band gap, electronic conductivity, elasticity, optical properties, etc.). So there is a unique ground state density $\rho(r)$ and a unique functional $F[\rho(r)]$ for all interactions, but unlike in Hartree-Fock not all energy expressions are known. Thus, in principle the electron density will be exact after total energy minimisation, but only if the Hamiltonian is correct. Being able to not only obtain a variety of physical properties of crystals from DFT but also to model the unique electron density $\rho(r)$ of large structures from first principles and to directly correlate the results with experimentally determined electron densities, e.g. by X-ray diffraction, makes the method particularly attractive. In the authors' view this access has caused the major breakthrough of the method in recent years.

An approach to self-consistently solve the electronic Schrödinger equation and to minimise the error of the energy expressions within DFT, in particular of the kinetic term, was given by Kohn and Sham [139] (1965) introducing the concept of a non-interacting reference system with Kohn-Sham single particle orbitals $\phi_i(\mathbf{r}, s)$, whose electron density equals the ground state density $\rho(r)$ of the interacting system. The Kohn-Sham orbitals are kept orthogonal as solutions to the single particle equation. The functional of the total energy:

$$E[\rho(\mathbf{r})] = -\frac{1}{2} \sum_{i=1}^N \langle \phi_i | \nabla^2 | \phi_i \rangle + \frac{1}{2} \sum_{i=1}^N \sum_{j=1}^N \iint d\mathbf{r}_1 d\mathbf{r}_2 |\phi_i(\mathbf{r}_1)|^2 \frac{1}{r_{12}} |\phi_j(\mathbf{r}_2)|^2 - \sum_{i=1}^N \int d\mathbf{r}_1 \sum_K \frac{Z_K}{r_{1K}} |\phi_i(\mathbf{r}_1)|^2 + E_{XC}[\rho(\mathbf{r})]$$

to be minimised includes the exact kinetic energy of the non-interacting reference system, the electron-electron coulomb interaction (distances r_{12}), the stabilising electron-nucleus attraction (nucleus charge Z , distances r_{1K}) and the exchange and correlation energy E_{XC} containing besides exchange and correlation also the self-interaction correction and the shortage in kinetic energy. The theory is exact up to this last functional which remains a challenge in today's DFT development with more and more sophisticated expressions and approximations tackling higher and higher levels of accuracy, e.g. in band gap description, effective mass prediction, magnetic coupling, van der Waals interactions, atomisation, ionisation and reaction energies, and structure prediction, just to mention a few.

Due to the decreased complexity by utilising a one-electron density $\rho(r)$, it is nowadays possible to model systems of many hundreds of atoms from first principles calculations. These methods transfer material science to a next quality stage in general and in the field of Li-ion batteries in particular, as was already indicated in the introduction. Critical battery properties are accessible through these methods as well, i.e. ionic conductivity, phase stability with intercalation, and influence of defects and dopants [140]. In this respect, migration barriers can be calculated, e.g. by means of NEB methods, with the advantage that there are no empirical parameter reliability issues. A comprehensive example can be found in [140]. The theoretical techniques have reached such maturity that they have recently started to be used to perform high-throughput computational search of materials [141]. Computationally even more demanding *ab initio* MD is capable to reliable include temperature effects into absolute conductivity parameters. By computing properties on large databases of thousands of potential electrode materials, researchers can identify the most promising compounds to be targeted by follow-up experimental work.

To date, DFT calculations are regularly performed in the optimisation and design of new materials, with demonstrations in a number of research fields, such as energy storage [142, 143], catalysis [144], energy conversion [145], pharmaceutical [146], and metallurgy [147]. The availability of large high-performance supercomputer infrastructures coupled with DFT, pre-/post-processing libraries [30, 31, 148, 149] and databases [29, 141, 150] provide the ingredients to compute thousands of compounds, augmenting the predicting capabilities of computational chemistry and materials science to search for new high-potential battery materials with improved energy density (both per mass and per volume) [151–156]. One strategy is to look for materials that can provide high cell voltages, but still lie within the practical stability windows of commercial electrolytes.

The marriage of computational materials science with computer informatics is often referred to as high-throughput (HT) calculations. Figure 14 shows an example of workflow implemented in the Materials Project initiative [141] which uses the python materials genomics (pymatgen) [148] to process the input files for calculations, post-process the output files, and analyse the results.

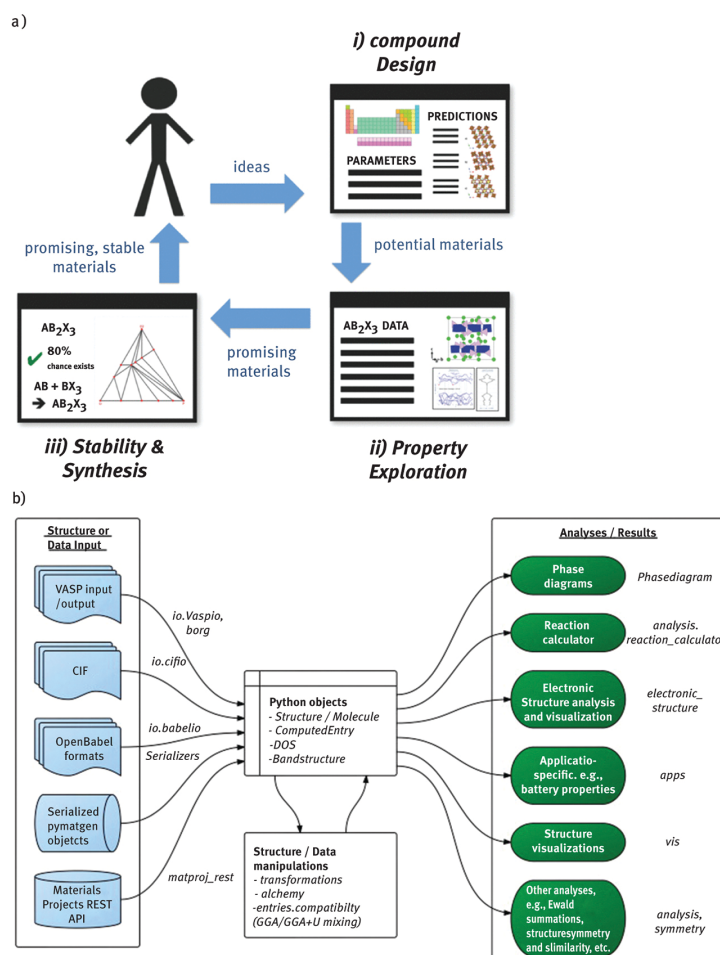


Figure 14: (a) Schematic of the workflow employed for performing high-throughput calculations and the resultant analysis in Materials Project (taken from [APL Materials 1, 011002 (2013)]; used in accordance with the Creative Commons Attribution (CC BY) license. (b) Structure of the python materials genomics (pymatgen) software which is used to power the Materials Project database taken from Ref. [148], (10.1016/j.commatsci.2012.10.028).

4.2 The materials project

The Materials Project aims to remove guesswork from materials design in a variety of applications by computing properties of all known materials [3]. Since 2011 a collaboration of leading researchers participates in this project in order to accelerate the computer-driven materials revolution [1]. The goal of this collaboration is to build free, open-access databases containing the fundamental thermodynamic and electronic properties of all known inorganic compounds. To date, basic properties of nearly all of the approximately 35,000 crystalline inorganic materials known to exist in nature were calculated as well as the properties of another few thousand that exist only in theory. Finally, with high-throughput DFT methods so far more than 67,000 inorganic compounds have been collected from which more than 3,600 are intercalation electrode materials and more than 16,100 are conversion type electrode materials for lithium-ion batteries. Different parameters can be accessed: structural (e.g. lattice parameters), electronic (e.g. voltage), and mechanical (e.g. elastic tensor). So far, more than 5,000 scientists have registered for access to the database containing this information. Thus, the experimental research can be targeted to the most promising compounds from computational data sets. It enables researchers to work out scientific trends in materials properties by data mining procedures.

In the following paragraphs, we discuss some of the properties accessible via high-throughput calculations in the field of materials for energy storage applications to go beyond experimental improvement of voltages in materials through modifying the materials composition, utilising well established rules of thumb, the so-called “chemical intuition”.

4.3 Open-circuit cell voltage

The open-circuit intercalation (conversion) voltage is set by the difference in the chemical potential, $\Delta\mu_X$, of the intercalation species (e.g. X = Li, Na, or Mg) in anode (e.g. Li metal in Li-ion batteries) and cathode material (e.g. LiCoO₂):

$$V = -\frac{[\mu_X^{\text{cathode}} - \mu_X^{\text{anode}}]}{zF}, \quad (2)$$

$$\bar{V} = -\frac{1}{zF} \int_{n_1}^{n_2} [\mu_X^{\text{cathode}} - \mu_X^{\text{anode}}] dn_X = -\frac{\Delta G_{\text{reaction}}}{(n_2 - n_1) zF}, \quad (3)$$

where F is the Faraday constant and z is the electron transfer number. Since the cell device operates at constant temperature and pressure, the change of Gibbs free energy is solely set by the change of X content Δn_X between the anode and cathode weighted by the respective μ_X [157]. Therefore, integrating eq. (2) over the intercalation reaction (e.g., $\text{Li}_{n_1}\text{CoO}_2 + (n_2 - n_1) \text{Li}^{\text{anode}} \rightarrow \text{Li}_{n_2}\text{CoO}_2$) furnishes the open-circuit voltage as function of the Gibbs free energy change of the redox reaction for delivering $n_2 - n_1$ equivalents of the intercalating species X. Note that eq. (3) is the basis of the well-known Nernst equation.

We note that DFT, in its various exchange-correlation functional flavours [139, 158–160] is limited only to internal ground state energies (and not free energies). Important thermal effects, such as configurational and vibrational entropy, are not captured. In general, at room temperature (and below), entropic and thermal contributions are negligible for many crystalline materials with high melting point, thus enabling us to approximate $\Delta G_{\text{reaction}}$ by $\Delta E_{\text{reaction}}$.

In DFT, the approximation of the exchange-correlation functional used can significantly vary redox reaction energetics and the predictability of open-circuit voltages. For example, the local density approximation (LDA) and the generalised gradient approximation (GGA) of the exchange-correlation fail to predict the intercalation voltages in highly correlated transition metal oxides due to spurious self-interaction errors [139, 158]. The self-interaction – the interaction of each electron with itself – underestimates the total energy of the reduced transition metal oxide, resulting in an underestimation of the intercalation voltage. In cathode materials with highly localised d or f electrons, such as LiFePO₄ and LiMn₂O₄, the self-interaction error becomes particularly important. Two strategies commonly used to improve the voltage prediction within DFT are adding an energy penalty in the form of a Hubbard U for specific orbital occupations (formally referred to as DFT + U) [160, 161], or adding a fraction of the exact Hartree-Fock exchange to the GGA exchange-correlation, as implemented in *hybrid functionals* [159, 162–166]. Since hybrid functionals are significantly more computationally expensive (at least, in the pseudopotential-planewave formalism) the DFT + U approach is commonly adopted in HT calculations. Previous studies have shown significant accuracy in DFT + U voltage predictions with respect to experimental observations [143]. A graphical summary of voltage calculations for battery materials is presented in Figure 15.

4.4 Dynamics of ions in energy storage materials

Apart from identifying cathode materials with high-energy densities, it remains equally important to identify cathodes and solid electrolytes with good intrinsic ionic transport. This is ultimately crucial in determining the power density of a given battery infrastructure [168, 169]. Particularly in the case of high-valent batteries, ionic mobility has been a major impediment in developing a wide range of cathode materials, as is available in Li-ion and Na-ion systems [170–172]. Typically, chemical intuition would suggest that ionic motion within “dense” or “close-packed” frameworks will be significantly poorer compared to “light” or “open” frameworks [173], but the most important factor for ionic diffusion is the chemical environment of the mobile ion and its evaluation during the migration process: even chemically “unfavourable” paths may show a flat energetic profile, if the environment stays “unfavourable” during the whole conduction path [174, 175], highlighting the non-intuitive behaviour of ionic motion and the importance of computations as a predictive tool for screening good candidates.

4.5 Ionic mobility

Ionic migration in periodic solids can be treated within the framework of transition state theory [176], a popular theoretical framework employed in the study of kinetics of chemical reactions (see Figure 16). Note that ions in solids will need to move via symmetrically equivalent sites, typically limited by a transition state with an energetic barrier, to ensure macroscopic diffusion. Given an energy barrier for migration (E_m), the diffusivity of a given ion in a solid is written in an Arrhenius equation (eq. (4)) as:

$$D = f a^2 v \exp\left(-\frac{E_m}{kT}\right), \quad (4)$$

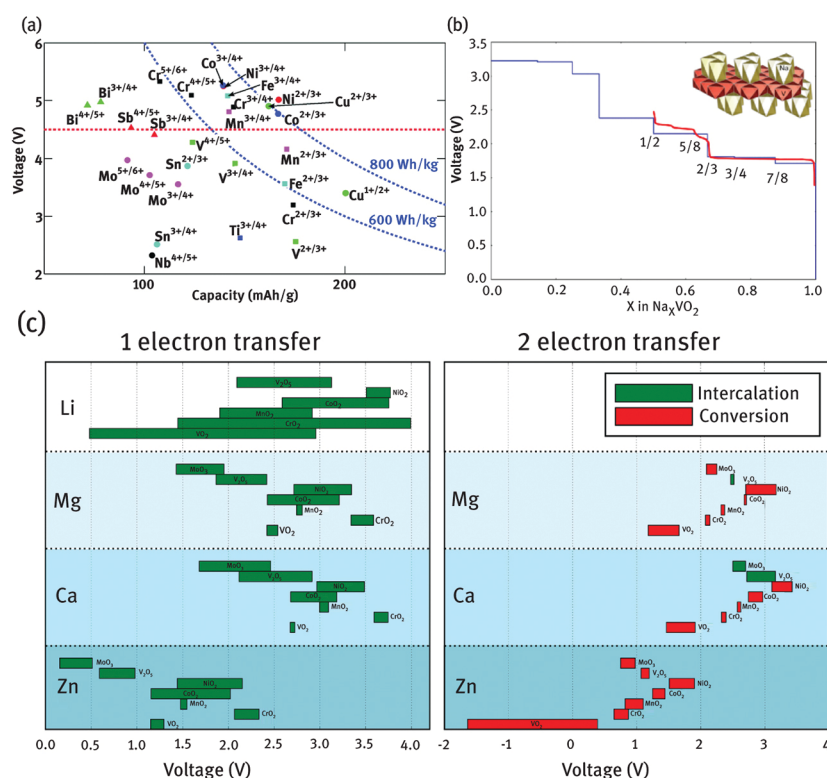


Figure 15: Examples of voltage calculations that have been applied to study the screening of several (a) Li intercalation in poly-anion materials as taken from Figure 4 of Ref. [156], (b) the benchmark of computed voltage curves against experiments for Na intercalation in VO_2 (Reprinted figure with permission from [167] [A. J. Toumar, S. P. Ong, W. Davidson Richards, S. Dacek, and G. Ceder, Physical Review Applied 4, 064002 (2015).] Copyright 2015 by the American Physical Society. <http://dx.doi.org/10.1103/PhysRevApplied.4.064002>), and (c) the competition of intercalation and conversion reactions in Li and multi-valent cathode materials (Reprinted from Chemical Reviews, 117, P. Canepa, G. S. Gautam, D. C. Hannah, R. Malik, M. Liu, K. G. Gallagher, K. A. Persson, and G. Ceder, Odyssey of Multivalent Cathode Materials: Open Questions and Future Challenges, 4287–4341, Copyright 2017, with permission from Elsevier, <http://pubs.acs.org/doi/abs/10.1021/acs.chemrev.6b00614>; further permissions related to the figure should be directed to the ACS).

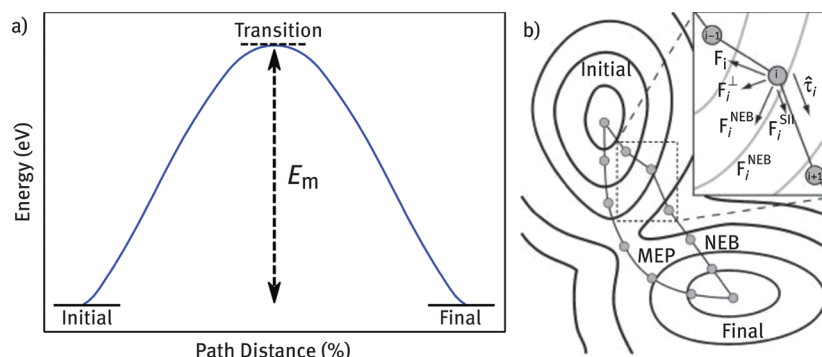


Figure 16: (a) Typical energy profile during ionic migration in a solid. The energy difference between the initial (and final) state and the transition state gives the energy barrier (E_m) for ionic migration. (b) Schematic of the force projection scheme used during the nudged elastic band minimisation scheme to find a minimum energy pathway (MEP) [179] (Reprinted from [D. Sheppard, R. Terrel, and G. Henkelman: “Optimization methods for finding minimum energy paths”, *The Journal of Chemical Physics* **128**, 134106 (2008).], with the permission of AIP Publishing).

where f , a , v , k , t indicate the correlation factor, distance between symmetrically equivalent sites, vibrational frequency, Boltzmann constant, and temperature, respectively [177]. Note that (E_m) is the most important intrinsic quantity that affects ionic diffusivity in a given solid and needs to be accurately determined, theoretically or experimentally. Also, the magnitude of (E_m) is dependent on the (accurately determined) energy difference between the transition state and the stable initial (or final) state (Figure 16).

The first step in calculating the energy of the transition state is accurately determining the transition state. Within the realm of ionic migration in solids, the transition state corresponds to a specific geometric position along the migration pathway, which is the saddle-point in the potential energy surface, i.e., the transition state is at an energy-maximum along the migration pathway but is also at an energy-minimum in comparison to other possible transition states (see Figure 16). While “slowest ascent” and “drag” methods have been used to determine transition states in chemical reactions before [32], the NEB method [179] has emerged as the most reliable theoretical framework to obtain precise transition states. The NEB method involves creating a “chain-of-states” or a discrete set of “images”, often referred to as a “band”, along the migration pathway and subsequently relaxing the band using a force projection scheme (Figure 16) [179]. Apart from accurately determining the transition state, the force projection in NEB facilitates the calculation of the energies along the images used to represent the migration pathway, which is useful to understand the migration mechanism.

While NEB is used to identify the transition state, DFT is nominally used to sample the potential energy surface (and related forces) within which the NEB is employed. Previous experimental studies have confirmed that DFT-based NEB can predict migration barriers with great accuracy, as illustrated in a variety of Li-ion, Na-ion, and Mg-ion conductors (and shown in Figure 17) [175, 180–186] and in a few Li-ion cathodes (such as LiFePO_4) [187].

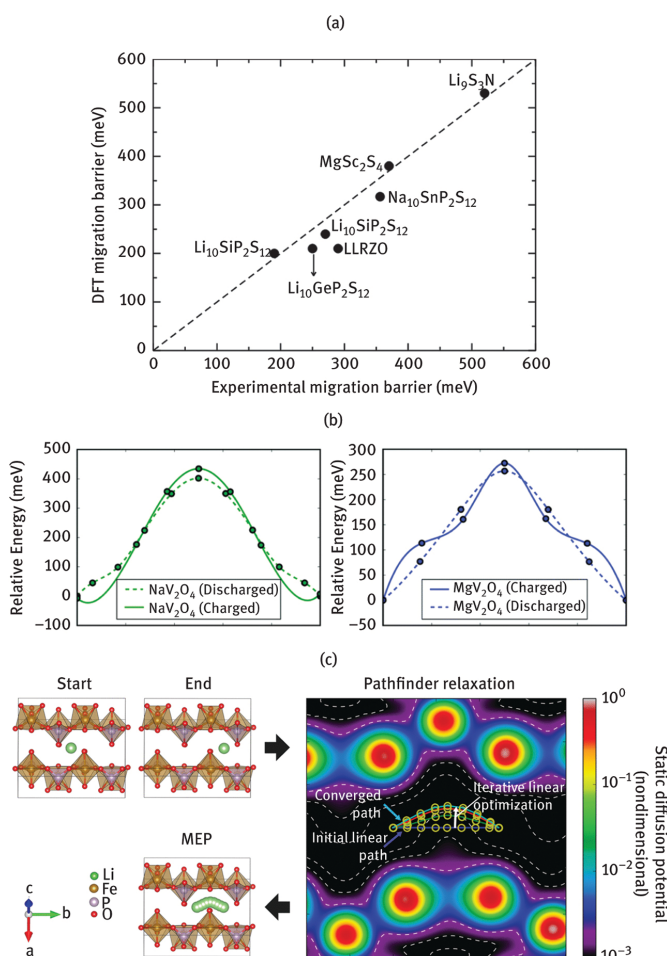


Figure 17: (a) Migration barriers calculated using DFT for various Li-ion, Na-ion, and Mg-ion conductors are plotted against corresponding barriers reported experimentally. LLRZO indicates $\text{Li}_{7.08}\text{La}_{2.96}\text{Rb}_{0.04}\text{Zr}_2\text{O}_{12}$. Dashed black line indicates parity. (b) Sample migration barrier calculations reported in NaV_2O_4 (green) and MgV_2O_4 (blue) post-spinel structures taken from Figure 3 of Ref. [193]. (Published by The Royal Society of Chemistry), which have also been investigated experimentally [194]. (c) Schematic of an electronic charge density based scheme to “speed up” the identification of the transition state using NEB, as demonstrated in the LiFePO_4 cathode [196].

Notably, in cathode systems which contain *d* or *f* transition metals with highly correlated electrons, DFT + *U* is normally used in voltage calculations to reduce self-interaction errors (as described above). However, previous studies have reported convergence difficulties in NEB calculations based on DFT + *U*, attributed to the metastability of the electronic states along the migration path [188–190]. During ionic migration in cathodes, the corresponding electron typically migrates across transition metal atoms, which is treated in adiabatic fashion within DFT + *U* due to the metastability of electron occupation, leading to poor convergence. In general, the barriers for electronic migration are lower compared to ionic migration in electrodes [162, 191], suggesting that the ionic migration is the rate-limiting step in cathodes, especially in high-valent systems [172, 188]. Also, previous studies that have indeed converged NEB calculations within DFT + *U* have reported insignificant differences in the barriers predicted versus DFT [192]. Recent experimental studies that qualitatively agree with DFT-NEB migration barrier predictions, especially in high-valent systems [189, 193–195], further validate the reliability of the DFT-NEB method.

Given the complexity of combining NEB and DFT, high-throughput studies that calculate migration barriers over hundreds of compounds are yet non-existent. Prior computational studies have relied on the identification of computationally inexpensive metrics or parameters that may be used to screen for fast ionic diffusers [144, 174]. Significant efforts have also been made in “accelerating” the identification of the transition state via better construction of the initial set of images used in the NEB [196], leading to the identification of a new class of potential high-valent cathodes [197]. Constructing a theoretical model, based on the NEB or otherwise, that allows for high-throughput calculations of migration barriers will eventually aid not only the battery community in the identification of new cathodes and ionic conductors but also in allied fields such as catalysis, fuel cells, and semi-conductors [144, 198].

If an ionic conduction model shall be investigated in dependence on temperature for a bulk material, the degrees of freedom of the electronic density distribution may be reduced to the utilisation of two- or three-particle potentials. This is realised by MD modelling which is described in the following.

5 Molecular dynamics

In MD, a trajectory is computed by iterative calculations of velocities and positions of a system in the future, one time increment apart from their values at a given time frame (Figure 18). In principle, a trajectory is set to visit any point in configuration space. In practice, large and possibly important regions thereof may remain unexplored within a typical, finite time MD simulation. While highly probable (*metastable*) regions are easily accessible, low probable regions may remain partially or even completely unsampled. Reasoning in terms of Gibbs free energy, if two metastable regions (state A and state B) are separated by high activation energy barriers ($\Delta G^\# \gg k_B T$), a trajectory will mostly linger in either A or B and only occasionally visit any intermediate region. Depending on the severity of the activation energy barrier, said regions may not be explored at all. This means that any activated process may pose a challenge to MD simulations, making it intrinsically difficult to explore microscopic mechanisms of any process containing free energy barriers.

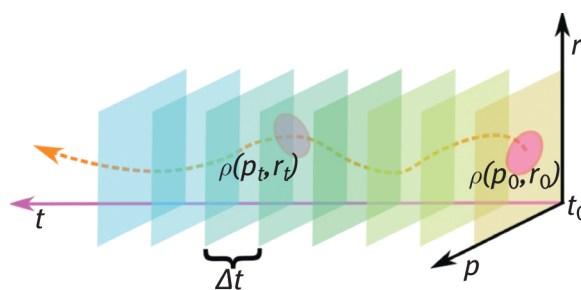


Figure 18: Trajectory (orange dashed line) computed in molecular dynamics simulation. Positions (r) and momenta (p) are propagated in finite time-steps (Δt).

Correctly describing ionic migration pathways within battery materials belongs to this class of problems. Different from purely diffusive processes, a cation-hopping from one site to an adjacent one implies overcoming internal free energy barriers. As pointed out in the last section, approaches based on total energy calculations as DFT or pair potentials [199, 200] can estimate energy barriers based on pathway-interpolations from site to site, followed by energy minimisation. Typical activation energies for the wide-spread battery material LiFePO₄ lie in the range (0.27–0.55) eV ([3133–6382] K) [199, 200]. In standard MD simulations, a significant overdriving of simulation parameters, here temperature would be required to sporadically observe inter-site particle (cation) jumps.

To address this problem related to the time scale of MD simulations, in recent years, different methods have focused on acceleration approaches. So-called collective variables (CV) were introduced [201, 202], as a means to selectively accelerate events, which would not occur in plain MD approaches. A CV represents a bundle of internal degrees of freedom of a system [203]. During an accelerated MD simulation, a CV markedly changes its value as a function of the progress of the simulation. In the example above, CV would have distinguishable values in state A and state B, and the progress of a CV-driven MD simulation would be marked by a sharp change of the CV value on moving from A to B. This approach has been successful in an increasing number of chemical systems from materials science to biological systems. For batteries though, the need to describe the collective motion of mobile cations within relatively rigid framework scaffoldings, makes the selection of efficient CVs less intuitive.

To efficiently collect details of cation jumping mechanisms, without overdriving temperature, the natural separation of frequencies between mobile, light cations and rigid, heavier framework atoms can be exploited. With the aim of elucidating pathways of cation (Li, Na) migration, our method [204] proceeds as follows: Instead of changing (overdriving) the overall temperature of the system, we “warm up” the mobile particles only by transferring a variable amount of kinetic energy from the slow (non-diffusive), heavier particles to the more mobile, lighter cations. For this purpose, velocity distributions are generated, which are not typical for the ensemble average, causing Li or Na cations to move quicker. As such, the chances of escaping local or global minima are increased. Along this line, the number of reactive events (jumps) is enhanced which results in shortened simulation times, lower nominal simulation temperature, and improved sampling efficiency [204].

A MD simulation accelerated this way can be implemented by introducing a perturbation of the velocities of each Li/Na cation at time t , by randomly choosing new values from a Gaussian distribution centred on

the actual velocity of the target atom. Therein, the warming up effect is achieved by broadening the Gaussian half-width. Perturbations are introduced under strict conservation of total linear and angular momenta. The perturbed snapshot is then propagated in MD simulations and the velocities are perturbed again at a later stage, until a sufficient number of events are collected [204].

After an initial latency, the system enters a regime where jumps are observed with a constant frequency, which allows for the estimation of mean paths and importance of different types of cation translocation modes.

Using this approach, a large statistic of jump events can be collected. In particular, collective events of cation translocation become accessible. This is different from approaches based on lattice energies, where single particle jumps are typically considered.

To illustrate the method, we compare the dynamics of particle translocation (Li and Na) in the olivine battery materials LiFePO_4 and NaFePO_4 . In Figure 19, splines are used to represent Li and Na displacements over a period of time of 500 ps. Correlated particle jumps are observed. The most common mechanistic pattern is represented by Li/Na migrations along the [010] channels, vertically in Figure 19. Episodically, jumps in the orthogonal direction [001], horizontally in Figure 19 are observed. This is an important result of considering collective cation dynamics, and is different from what can be predicted based on lattice energy calculations only. Indeed, [001] jumps were indicated elsewhere as “forbidden” [200], due to a too demanding activation energy barrier. However, thanks to collective movements, proximity of another charged particle can accelerate (i.e. catalyse) Li or Na jumps. Otherwise demanding barriers can be crossed this way.

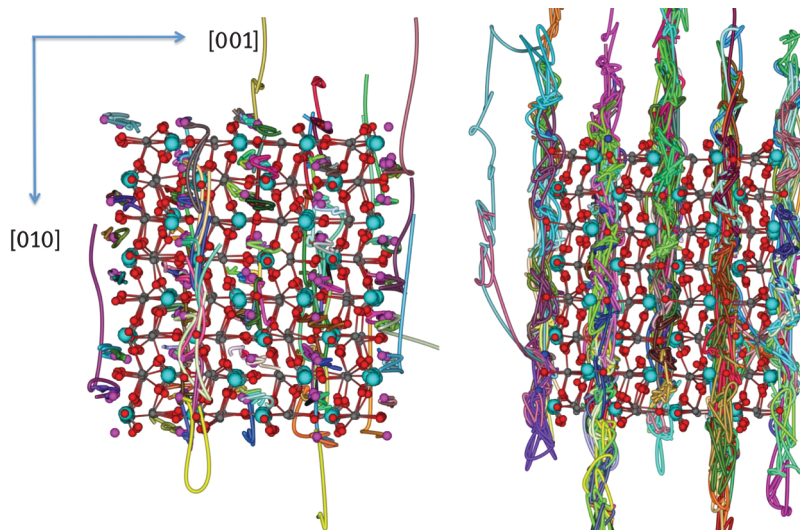


Figure 19: Displacements of Li and Na cations in the olivine materials LiFePO_4 (left) and NaFePO_4 (right), respectively. The Li/Na motions are represented as splines over a period of 500 ps ($T = 600$ K). While events of cation translocation are more frequent along [010], the easy olivine axis, jumps along [001] are part of the overall mechanism.

This approach is extremely valuable towards collecting mechanisms of cation translocation within battery materials, both existing and predicted. In existing materials, MD results can indicate relevant pathways along which cations actually move. Combined with different techniques (Umbrella sampling, kinetic MC), rate constants and diffusion constants can be reliably calculated, subsequently. This provides a very solid basis for the prediction of cation translocation efficiency in predicted battery materials.

Migration paths as predicted from the VDP and BVSE methodologies can be weighted according to the probability of cation migration along different pathways.

6 Summary

Crystallography is a powerful tool for the analysis of (crystalline) solid-state materials. Since the model of diffusion can be described very well by crystallographic means, the electrochemical processes in batteries and accumulators concerning the energy conversion from chemical to electrical energy can be described, as well. This way, new materials can be predicted with promising electrochemical functions. We presented a new methodology that seeks to optimise the time-efficiency of such a search by first utilising computationally less expensive approaches and applying increasingly complex calculations to these resulting promising materials. We have focussed on Voronoi-Dirichlet partitioning, a method analysing solely the geometry of crystal structure; BVSE calculations, combining the static crystal structure geometry with energetic parameters based on data mining;

density functional theoretical simulations to evaluate the principal diffusion step(s) *ab initio*; and MD simulations to model the dynamics of the ion conduction. In this order, fewer crystal structures are calculated with more time-consuming methodologies that allow gathering more in-depth information based on energetic parameters.

Crystallographic databases like the ICSD, CSD, and the PCD represent a growing and increasingly reliable foundation for data mining, big-data approaches, and machine-learning. The more and the better the data collected within, the more promising functional materials may be identified, since the probability to find compounds with those crystallographic features necessary for high ionic diffusivity is increasing with the amount of reported crystal structures in crystallographic databases.

In the very near future, materials scientists will use high-throughput computing together with big-data approaches, topological methods, and database screening for identifying and designing novel best-suited materials and complete battery systems. The authors of this contribution follow the view of G. Ceder [1], who already stated “that this will lead to technologies that will reshape our world – breakthroughs that will transform computing, eliminate pollution, generate abundant clean energy and improve our lives in ways that are hard to imagine today”.

Acknowledgements

FM, TN, MZ, TL, and DCM are grateful for financial support of the Federal Ministry of Education and Research (CryPhysConcept (03EK3029A) and R2RBattery (03SF0542A)). PC is grateful to the Ramsey Memorial Trust for the provision of his Ramsey Fellowship. SL acknowledges support from the UK Research Council for using work in the paper that was undertaken by a student under Project No. EP/M50631X/. SL also thanks ARCCA Cardiff for computational resources. SA would like to thank National Research Foundation, Prime Minister’s Office, Singapore for support under its Competitive Research Programme (NRF-CRP 10-2012-6) and NUS for support under the “NUS Centre for Energy Research” grant. VAB is grateful for financial support of the Russian Megagrant (14.B25.31.0005), and the Russian Science Foundation (16-13-10158).

Notes

1 As stated in [1, 3], the Massachusetts Institute of Technology has found that the commercialisation of a successful material from lab-scale takes an average of 15–20 years. This long and resource-tying process costs companies and research institutes billions of US Dollars [1]. High-throughput computational materials design is capable to dramatically reduce costs and time spent on this.

2 In the scientific literature, the term *multivalent* is widely spread. We propose to avoid this term since it originally meant ions of multiple valence states (such as Cr). A synonym would be polyvalent. We suggest the term *high-valent* or *highly valent* and use it in this manuscript. Many high-valent cations are also multivalent but cations mostly regarded for future electrochemical energy storage devices are not multivalent (in this sense), like Al or Mg.

3 The rhombohedral (trigonal) structure of $\text{Li}_{0.5}\text{CoO}_2$, for instance, was first described in 1958 in Ref. [205], according to the datasets found within the Inorganic Crystal Structure Database (ICSD) [79]. This material was investigated regarding its magnetic properties, elucidating the concept of double-exchange interaction. The structure was already well-known but put in a very different context in 1980 – 22 years later – when it was first proposed as an interesting positive electrode candidate by the group of John B. Goodenough [206]. For LiFePO_4 the numbers are even further apart. Its use for Li-ion batteries was first proposed in 1997, again by the group of John B. Goodenough [207] but the material itself is already known as a mineral since 1834 [208]. J. N. Fuchs even obtained Li from this mineral through acidic dissolution 1 year later [209]. According to the datasets in the ICSD, the structure was first solved in 1938 [210] whereas the first synthesised structure is from 1977 [211].

4 For computation of Voronoi-Dirichlet partitioning, a faster and more efficient “gift wrapping” algorithm is used [65].

5 ToposPro is available for free at <http://topospro>.

6 Duplicates share the same space group, number of atoms, composition, and unit cell volume.

7 This is a comparison between the recorded chemical composition of the cif-file and the composition calculated from the occupancies and multiplicities of the atomic sites (of each occupied crystallographic orbit).

References

- [1] Ceder G, Persson K. The Stuff of Dreams. *Sci Am.* 2013;309:36–40
- [2] Strategische weiterentwicklung des hoch- und höchstleistungsrechnens in Deutschland. Germany: Deutscher Wissenschaftsrat, 2012
- [3] Fueling discovery by sharing. *Nat Mater.* 2013;12:173. DOI: 10.1038/nmat3594.
- [4] Material’s Project, <https://materialsproject.org>, cited 04.05.2017.
- [5] ‘Partnership for Advanced Computing in Europe’, <http://www.prace-ri.eu> (cited 09. March 2017).
- [6] Boosting materials modelling. *Nat Mater.* 2016;15:365. DOI: 10.1038/nmat4619.
- [7] Jahan A, Ismail MY, Sapuan SM, Mustapha F. Material screening and choosing methods – a review. *Mater Des.* 2010;31:696–705.

- [8] Mayr LM, Bojanic D. Novel trends in high-throughput screening. *Curr Opin Pharmacol.* 2009;9:580–588.
- [9] Green ML, Choi CL, Hattrick-Simpers JR, Joshi AM, Takeuchi I, Barron SC, et al. Fulfilling the promise of the materials genome initiative with high-throughput experimental methodologies. *Appl Phys Rev.* 2017;4:011105.
- [10] Levi E, Levi MD, Chasid O, Aurbach D. A review on the problems of the solid state ions diffusion in cathodes for rechargeable Mg batteries. *J Electroceram.* 2009;22:13–9.
- [11] Elia GA, Marquardt K, Hoeppner K, Fantini S, Lin R, Knipping E, et al. An overview and future perspectives of aluminum batteries. *Adv Mater.* 2016;28:7564–79.
- [12] Van Noorden R. The rechargeable revolution: a better battery. *Nature.* 2014;507:26–8.
- [13] ‘Company overview of Pellion Technologies Inc.’, Bloomberg. Available at: <http://www.bloomberg.com/research/stocks/private/snapshot.asp?privcapId=114339859>. Accessed: 04 May 2017.
- [14] Anurova NA, Blatov VA, Ilyushin GD, Blatova OA, Ivanov-Schitz AK, Dem’yanets LN. Migration maps of Li⁺ cations in oxygen-containing compounds. *Solid State Ionics.* 2008;179:2248–54.
- [15] Hautier G, Fischer C, Ehrlacher V, Jain A, Ceder G. Data mined ionic substitutions for the discovery of new compounds. *Inorg Chem.* 2011;50:656–63.
- [16] Avdeev M, Sale M, Adams S, Rao RP. Screening of the alkali-metal ion containing materials from the Inorganic Crystal Structure Database (ICSD) for high ionic conductivity pathways using the bond valence method. *Solid State Ionics.* 2012;225:43–6.
- [17] Gao J, Chu G, He M, Zhang S, Xiao R, Li H, Chen L. Screening possible solid electrolytes by calculating the conduction pathways using bond valence method. *Sci China Phys Mech Astron.* 2014;57:1526–36.
- [18] Xiao R, Li H, Chen L. High-throughput design and optimization of fast lithium ion conductors by the combination of bond-valence method and density functional theory. *Sci Rep.* 2015;5:14227.
- [19] Meutzner F, Münchgesang W, Leisegang T, Schmid R, Zschornak M, Ureña De Vivanco M, Shevchenko AP, Blatov VA, Meyer DC. Identification of solid oxygen-containing Na-electrolytes: an assessment based on crystallographic and economic parameters. *Crystal Res Technol.* 2017;52:1600223.
- [20] Wang Y, Richards WD, Ong SP, Miara LJ, Kim JC, Mo Y, Ceder G. Design principles for solid-state lithium superionic conductors. *Nat Mater.* 2015;14:1026–31.
- [21] Wong LL, Chen H, Adams S. Design of fast ion conducting cathode materials for grid-scale sodium-ion batteries. *Phys Chem Chem Phys.* 2017;19:7506–23.
- [22] Data mining, Merriam Webster: <https://www.merriam-webster.com/dictionary/data%20mining> (cited 04.05.2017).
- [23] Larose DT. Discovering knowledge in data: an introduction to data mining. Hoboken, NJ: Wiley & Sons Inc., 2014.
- [24] Sendek AD, Yang Q, Cubuk ED, Duerloo K-A, Cui Y, Reed EJ. Holistic computational structure screening of more than 12000 candidates for solid lithium-ion conductor materials. *Energy Environ Sci.* 2017;10:306–20.
- [25] Manyika J, Chui M, Brown B, Bughin J, Dobbs R, Roxburgh C, et al. Big data: the next frontier for innovation, competition, and productivity. Brussels, San Francisco: McKinsey Global Institute, McKinsey & Company, 2011.
- [26] Qu X, Jain A, Rajput NN, Cheng L, Zhang Y, Ong SP, et al. The electrolyte genome project: a big data approach in battery materials discovery. *Comput Mater Sci.* 2015;103:56–67.
- [27] Meutzner F, Münchgesang W, Kabanova NA, Zschornak M, Leisegang T, Blatov VA, Meyer DC. On the way to new possible Na-ion conductors: the Voronoi–Dirichlet approach, data mining and symmetry considerations in ternary Na oxides. *Chem – Eur J.* 2015;21:16601–8.
- [28] Ghadbeigi L, Sparks TD, Harada JK, Lettieri BR. Data-mining approach for battery materials. 2015 IEEE Conference on Technologies for Sustainability (SusTech), 2015:239–44.
- [29] Hachmann J, Olivares-Amaya R, Atahan-Evrink S, Amador-Bedolla C, Sánchez-Carrera RS, Gold-Parker A, Vogt L, Brockway AM, Aspuru-Guzik A. The Harvard clean energy project: large-scale computational screening and design of organic photovoltaics on the world community grid. *J Phys Chem Lett.* 2011;2:2241–51.
- [30] Curtarolo S, Setyawan W, Wang S, Xue J, Yang K, Taylor RH, et al. AFLOWLIB. ORC: a distributed materials properties repository from high-throughput ab initio calculations. *Comput Mater Sci.* 2012;58:227–35.
- [31] Saal JE, Kirklin S, Aykol M, Meredig B, Wolverton C. Materials design and discovery with high-throughput density functional theory: the open quantum materials database (OQMD). *Jom.* 2013;65:1501–9.
- [32] Jónsson H, Mills G, Jacobsen KW. Nudged elastic band method for finding minimum energy paths of transitions. In: Berne BJ, Ciccotti G, Coker DF, editor(s). Classical and quantum dynamics in condensed phase simulations. Singapore, New Jersey, London, Hong Kong: World Scientific, 1998:385–404.
- [33] Adams S, Swenson J. Predictability of ion transport properties from the structure of solid electrolytes. *Ionics.* 2004;10:317–26.
- [34] Adams S. Modelling ion conduction pathways by bond valence pseudopotential maps. *Solid State Ionics.* 2000;136:1351–61.
- [35] Ling S-G, Gao J, Xiao R-J, Chen L-Q. High-throughput theoretical design of lithium battery materials. *Chin Phys B.* 2016;25:018208.
- [36] Xiao R, Li H, Chen L. Candidate structures for inorganic lithium solid-state electrolytes identified by high-throughput bond-valence calculations. *J Materomics.* 2015;1:325–32.
- [37] Adams S, Prasada Rao R. Transport pathways for mobile ions in disordered solids from the analysis of energy-scaled bond-valence mismatch landscapes. *Phys Chem Chem Phys.* 2009;11:3210–6.
- [38] Adams S, Prasada Rao R. Understanding ionic conduction and energy storage materials with bond-valence-based methods. In: Brown ID, Poeppelmeier KR, editor(s). Bond Valences. Berlin Heidelberg: Springer, 2014:129–59.
- [39] Sale M, Avdeev M. 3DBVSMAPPER: a program for automatically generating bond-valence sum landscapes. *J Appl Crystallogr.* 2012;45:1054–6.
- [40] Filsø MØ, Turner MJ, Gibbs GV, Adams S, Spackman MA, Iversen BB. Visualizing lithium-ion migration pathways in battery materials. *Chem – Eur J.* 2013;19:15535–44.
- [41] Filsø MØ, Eikeland E, Iversen BB. Procrystal analysis as a tool for the visualization of ion migration pathways. *AIP Conference Proceedings* 2016;1765:020010.

- [42] Adams S, Swenson J. Determining ionic conductivity from structural models of fast ionic conductors. *Phys Rev Lett.* 2000;84:4144.
- [43] Adams S, Swenson J. Bond valence analysis of transport pathways in RMC models of fast ion conducting glasses. *Phys Chem Chem Phys.* 2002;4:3179–84.
- [44] Adams S, Swenson J. Bond valence analysis of reverse Monte Carlo produced structural models; a way to understand ion conduction in glasses. *J Phys Condens Matter.* 2005;17:S87–101.
- [45] Müller C, Zienicke E, Adams S, Habasaki J, Maass P. Comparison of ion sites and diffusion paths in glasses obtained by molecular dynamics simulations and bond valence analysis. *Phys Rev B.* 2007;75:014203.
- [46] Cai L, White RE. Mathematical modeling of a lithium ion battery with thermal effects in COMSOL Inc. Multiphysics (MP) software. *J Power Sources.* 2011;196:5985–9.
- [47] COMSOL Multiphysics® 3.5a USER'S Guide. 2008a. COMSOL Inc.
- [48] COMSOL Multiphysics® 3.5a Reference Guide. 2008b. COMSOL Inc.
- [49] Takada K, Ohno T. Experimental and computational approaches to interfacial resistance in solid-state batteries. *Front Energy Res.* 2016;4:10.
- [50] In: Meyer DC, Leisegang T, editor(s). *Electrochemical storage materials: from crystallography to manufacturing technology.* OLDENBOURG: DE GRUYTER Publishing House, 2018
- [51] Nishijima M, Ootani T, Kamimura Y, Sueki T, Esaki S, Murai S, et al. Accelerated discovery of cathode materials with prolonged cycle life for lithium-ion battery. *Nat Commun.* 2014;5:4553.
- [52] Fuess H, Hahn T, Wondratschek H, Müller U, Shmueli U, Prince E, et al., editors. *International tables for crystallography.* Berlin: Springer, 2004.
- [53] Batten SR, Robson R. Interpenetrating nets: ordered, periodic entanglement. *Angew Chemie Int Ed.* 1998;37:1460–94.
- [54] Blatov VA, Shevchenko AP, Proserpio DM. Applied topological analysis of crystal structures with the program package ToposPro. *Cryst Growth Des.* 2014;14:3576–86.
- [55] Blatov VA, Proserpio DM. Periodic-graph approaches in crystal structure prediction. In: Oganov AR, editor(s). *Modern methods of crystal structure prediction.* Weinheim: Wiley VCH, 2011:1–28.
- [56] Frank FT, Kasper J. Complex alloy structures regarded as sphere packings. I. Definitions and basic principles. *Acta Crystallogr.* 1958;11:184–90.
- [57] Frank FT, Kasper J. Complex alloy structures regarded as sphere packings. II. Analysis and classification of representative structures. *Acta Crystallogr.* 1959;12:483–99.
- [58] O'Keeffe M, Hyde BG. *Crystal structures I. Patterns and symmetry.* Washington, DC: Mineralogical Society of America, 1996.
- [59] Steurer W, Dshemuchadse J. *Intermetallics: structures, properties, and statistics.* Oxford: Oxford University Press, International Union of Crystallography Monographs on Crystallography, 2016
- [60] Aurenhammer F. Voronoi diagrams – a survey of a fundamental geometric data structure. *ACM Comput Surv.* 1991;23:345–405.
- [61] Voronoi GF. Nouvelles applications des paramètres continus à la théorie des formes quadratiques. Deuxième mémoire. Recherches sur les paralléloèdres primitifs. *J Reine Angew Math.* 1908;134:198–287.
- [62] Dirichlet GL. Über die Reduktion der positiven quadratischen Formen mit drei unbestimmten ganzen Zahlen. *J Reine Angew Math.* 1850;40:209–27.
- [63] Niggli P. Die topologische Strukturanalyse. I. Z. Kristallogr Cryst Mater. 1927;65:391–415.
- [64] Blatov VA, Shevchenko AP, Serenzhkin VN. Crystal space analysis by means of Voronoi–Dirichlet polyhedra. *Acta Crystallogr A.* 1995;51:909–16.
- [65] Blatov VA. Voronoi–Dirichlet polyhedra in crystal chemistry: theory and applications. *Crystallogr Rev.* 2004;10:249–318.
- [66] Descartes R. *Principia philosophiae.* Amsterdam: Apud Ludovicum Elzevirum, 1644.
- [67] Liebling TM, Pourdin L. Voronoi diagrams and Delaunay triangulations: ubiquitous Siamese twins. *Doc Math Extra Volume Optim Stories.* 2012;2012:419–31.
- [68] Blatov VA, Serezhkin VN. Stereoatomic model of the structure of inorganic and coordination compounds. *Russ J Inorg Chem.* 2000;45:S105–22.
- [69] Voroglide. Fernuni Hagen. <http://www.pi6.fernuni-hagen.de/GeomLab/VoroGlide>. Accessed 01 Mar 2017.
- [70] Blatov VA, Ilyushin GD, Blatova OA, Anurova NA, Ivanov-Schits AK, Dem'yanets LN. Analysis of migration paths in fast-ion conductors with Voronoi–Dirichlet partition. *Acta Crystallogr B.* 2006;62:1010–8.
- [71] Blatov VA, Shevchenko AP. Registration of the computer program 'ToposPro', Russian certificate No. 2013619016, 2013.
- [72] Global materials market for alternative energy storage mechanisms. Frost & Sullivan, 2011:9833–9.
- [73] Buss K, Wrobel P, Doetsch C. Global distribution of grid connected electrical energy storage systems. *Int J Sustainable Energy Plann Manag.* 2016;9:31–56.
- [74] Kummer JT, Neill W. Battery having a molten alkali metal anode and a molten sulfur cathode. Publication date: 26. November 1968, US Patent US3413150 A.
- [75] Yao Y-F, Kummer JT. Ion exchange properties of and rates of ionic diffusion in beta-alumina. *J Inorg Nucl Chem.* 1967;29:2453–75.
- [76] Hueso KB, Armand M, Rojo T. High temperature sodium batteries: status, challenges and future trends. *Energy Environ Sci.* 2013;6:734–49.
- [77] Daniel C, Besenhard J. *Handbook of battery materials*, vol. 1, 2nd ed. Weinheim: Wiley-VCH; 2011.
- [78] Dunn B, Kamath H, Tarascon JM. Electrical energy storage for the grid: a battery of choices. *Sci.* 2011;334:928–35.
- [79] Belsky A, Hellenbrandt M, Karen VL, Luksch P. New developments in the inorganic crystal structure database (ICSD): accessibility in support of materials research and design. *Acta Crystallogr B.* 2002;58:364–9.
- [80] Whittingham MS, Huggins RA. Measurement of sodium ion transport in beta alumina using reversible solid electrodes. *J Chem Phys.* 1971;54:414–6.
- [81] Song S, Duong HM, Korsunsky AM, Hu N, Lu L. A Na⁺ superionic conductor for room-temperature sodium batteries. *Sci Rep.* 2016;6:32330.

- [82] Beyeler HU, Shannon RD, Chen HY. Ionic conductivity of single-crystal $\text{Na}_5\text{YSi}_4\text{O}_{12}$. *Appl Phys Lett.* 1980;37:934–5.
- [83] Glöser S, Espinoza LT, Ganderberger C, Faulstich M. Raw material criticality in the context of classical risk assessment. *Resour Policy.* 2015;44:35–46.
- [84] Brown ID, Poepelmeier KR, editors. *Bond valences*. Berlin Heidelberg: Springer, 2014.
- [85] Pauling L. The principles determining the structure of complex ionic crystals. *J Am Chem Soc.* 1926;51:1010–26.
- [86] Brown ID. Recent developments in the methods and applications of the bond valence model. *Chem Rev.* 2009;109:6858–919.
- [87] Baur WH. Bond length variation and distorted coordination polyhedra in inorganic crystals. *Trans Am Crystallogr Assoc.* 1970;6:125–55.
- [88] Donnay G, Allmann R. How to recognize O^{2-} , OH^- , and H_2O in crystal structures determined by X-rays. *Am Mineral.* 1970;55:1003–15.
- [89] Brown ID, Altermatt D. Bond-valence parameters obtained from a systematic analysis of the inorganic crystal structure database. *Acta Crystallogr B.* 1970;41:244–7.
- [90] Adams S. From bond valence maps to energy landscapes for mobile ions in ion-conducting solids. *Solid State Ionics.* 2006;177:1625–30.
- [91] Preiser C, Loesel J, Brown ID, Kunz M, Skowron A. Long-range Coulomb forces and localized bonds. *Acta Crystallogr B.* 1999;55:698–711.
- [92] Brown ID. The chemical bond in inorganic chemistry: the bond valence model. Oxford: Oxford University Press, 2002:27.
- [93] Garrett JD, Greedan JE, Faggiani R, Carbotte S, Brown ID. Single-crystal growth and structure determination of $\text{Ag}_{16}\text{I}_{12}\text{P}_2\text{O}_7$. *J Solid State Chem.* 1982;42:183–90.
- [94] Zhou Y, Adams S, Rao RP, Edwards DD, Neiman A, Pestereva N. Charge transport by polyatomic anion diffusion in $\text{Sc}_2(\text{WO}_4)_3$. *Chem Mater.* 2008;20:6335–45.
- [95] Yashima M, Sekikawa T, Sato D, Nakano H, Omoto K. Crystal structure and oxide-ion diffusion of nanocrystalline, compositionally homogeneous ceria–zirconia $\text{Ce}_{0.5}\text{Zr}_{0.5}\text{O}_2$ up to 1176K. *Cryst Growth Des.* 2013;13:829–37.
- [96] Cabana J, Ling CD, Oró-Solé J, Gautier D, Tobias G, Adams S, Canadell E, Palacin MR. Antifluorite-type lithium chromium oxide nitrides: synthesis, structure, order, and electrochemical properties. *Inorg Chem.* 2004;43:7050–60.
- [97] Mazza D. Modeling ionic conductivity in Nasicon structures. *J Solid State Chem.* 2001;156:154–60.
- [98] Fedotov SS, Kabanov AA, Kabanova NA, Blatov VA, Zhugayevych A, Abakumov AM, Khasanova NR, Antipov EV. Crystal structure and Li-ion transport in $\text{Li}_2\text{CoPO}_4\text{F}$ high-voltage cathode material for Li-ion batteries. *J Phys Chem C.* 2017;121:3194–202.
- [99] Ouerfelli N, Guesmi A, Mazza D, Madani A, Zid MF, Driss A. Synthesis, crystal structure and mono-dimensional thallium ion conduction of $\text{TiFe}_{0.22}\text{Al}_{0.78}\text{As}_2\text{O}_7$. *J Solid State Chem.* 2007;180:1224–9.
- [100] Safanama D, Sharma N, Rao RP, Brand HE, Adams S. Structural evolution of NASICON-type $\text{Li}_{1+x}\text{Al}_x\text{Ge}_{2-x}(\text{PO}_4)_3$ using in situ synchrotron X-ray powder diffraction. *J Mater Chem A.* 2006;4:7718–26.
- [101] Kan WH, Huq A, Manthiram A. Exploration of a metastable normal spinel phase diagram for the quaternary Li–Ni–Mn–Co–O system. *Chem Mater.* 2016;28:1832–7.
- [102] Adams S. Relationship between bond valence and bond softness of alkali halides and chalcogenides. *Acta Crystallogr B.* 2001;57:278–87.
- [103] Chen H, Adams S. Bond softness sensitive bond-valence parameters for crystal structure plausibility tests. *IUCrJ.* 2017;4:614–25.
- [104] Swenson J, Adams S. Application of the bond valence method to reverse Monte Carlo produced structural models of superionic glasses. *Phys Rev B.* 2001;64:024204.
- [105] Swenson J, Adams S. Mixed alkali effect in glasses. *Phys Rev Lett.* 2003;90:155507.
- [106] Hall A, Swenson J, Adams S, Meneghini C. Mixed mobile ion effect and cooperative motions in silver-sodium phosphate glasses. *Phys Rev Lett.* 2008;101:195901.
- [107] Adams S, Rao RP. High power lithium ion battery materials by computational design. *Phys Status Solidi A.* 2011;208:1746–53.
- [108] Adams S, Rao RP. Structural requirements for fast lithium ion migration in $\text{Li}_{10}\text{GeP}_2\text{S}_{12}$. *J Mater Chem.* 2012;22:7687–91.
- [109] Wong LL, Chen HM, Adams S. Sodium-ion diffusion mechanisms in the low cost high voltage cathode material $\text{Na}_{2+\delta}\text{Fe}_{2-\delta/2}(\text{SO}_4)_3$. *Phys Chem Chem Phys.* 2015;17:9186–93.
- [110] Nishitani Y, Adams S, Ichikawa K, Tsujita T. Evaluation of magnesium ion migration in inorganic oxides by the bond valence site energy method. *Solid State Ionics.* 2018;315:111–115.10.1016/j.ssi.2017.11.031.
- [111] Wong LL, Chen H, Adams S. Design of fast ion conducting cathode materials for grid-scale sodium-ion batteries. *Physical Chemistry Chemical Physics.* 2017;19:7506–7523.10.1039/C7CP00037E.
- [112] Pearson WH, Lomax JF. X-ray crystal diffraction study of Zr, Na-beta -alumina. *Mate Res Soc Symp Proc.* 1993;293:315–21.
- [113] Boilot JP, Collin G, Colombar P. Relation structure-fast ion conduction in the NASICON solid solution. *J Solid State Chem.* 1988;73:160–71.
- [114] Collin G, Comes R, Boilot JB, Colombar P. Disorder of tetrahedra in Nasicon-type structure – Part I. $\text{Na}_3\text{Sc}_2(\text{PO}_4)_3$: structures and ion-ion correlations. *J Phys Chem.* 1986;47:843–54.
- [115] Susman S, Delbecq CJ, Brun TO, Prince E. Fast ion transport in the Nasicon analog $\text{Na}_3\text{Sc}_2(\text{PO}_4)_3$: structure and conductivity. *Solid State Ionics.* 1983;9:839–44.
- [116] Chamkir M, El Jazouli A, De Waal D. Synthesis, crystal structure and spectroscopy properties of $\text{Na}_3\text{AZr}(\text{PO}_4)_3$ ($\text{A} = \text{Mg, Ni}$) and $\text{Li}_{2-\epsilon}\text{Na}_{0.4}\text{NiZr}(\text{PO}_4)_3$ phosphates. *J Solid State Chem.* 2006;179:1883–91.
- [117] Zatrosky IV. NASICON-type $\text{Na}_3\text{V}_2(\text{PO}_4)_3$. *Acta Crystallogr E.* 2010;66:pi12–12.
- [118] Maksimov BA, Belov NV. The high temperature X-ray analysis of the monocrystals $\text{Na}_5\text{YSi}_4\text{O}_{12}$. *Dokl Akad Nauk SSSR.* 1981;261:623–7.
- [119] Rüscher CH, Gesing TM, Buhl J-C. Anomalous thermal expansion behaviour of $\text{Na}_8[\text{AlSiO}_4]_6(\text{NO}_3)_2$ -sodalite: P43n to Pm3n phase transition by untilting and contraction of TO_4 units. *Z Kristallogr Cryst Mater.* 2003;218:332–44.
- [120] Barth TF, Posnjak E. Silicate structures of the cristobalite type: III. Structural relationship of high-cristobalite, alpha-carnegieite, and Na_2SiO_4 . *Z Kristallogr.* 1932;81:376–85.
- [121] Baur WH, Joswig W. The phases of natrolite occurring during dehydration and rehydration studied by single crystal X-ray diffraction methods between room temperature and 923 K. *Neues Jahrb Mineral Abh Monatsh.* 1996;1996:171–87.
- [122] Kahlenberg V, Böhm H. Crystal structure of hexagonal trinepheline – a new synthetic NaAlSiO_4 modification. *Am Mineral.* 1998;83:631–7.

- [123] Isasi J, Daidouh A. Synthesis, structure and conductivity study of new monovalent phosphates with the langbeinite structure. *Solid State Ionics*. 2000;133:303–13.
- [124] Williams JJ, Smith CW, Evans KE, Lethbridge ZA, Walton RI. Off-axis elastic properties and the effect of extraframework species on structural flexibility of the NAT-type zeolites: simulations of structure and elastic properties. *Chem Mater*. 2007;19:2423–34.
- [125] Saniz R, Freeman AJ. Pressure effects on the electronic properties and superconductivity of the beta-pyrochlore oxides: AO_3O_6 ($\text{A} = \text{Na}$, K , Rb , Cs). *Phys Rev B*. 2007;72:024522.
- [126] Nishi F, Takuechi Y. Cubic structure of sodium calcium germanate $\text{Na}_{3.7}\text{Ca}_{1.15}\text{Ge}_3\text{O}_9$. *Acta Crystallogr C*. 1988;44:1867–9.
- [127] Michiue Y, Watanabe M. $\text{Na}_x\text{Cr}_x\text{Ti}_{8-x}\text{O}_{16}$, priderite with sodium ions in the tunnel structural study for stability and Na ion transport. *J Solid State Chem*. 1995;116:269–99.
- [128] Vuli P, Kahlenberg V. On the high temperature behaviour of monoclinic trinepheline. *Neues Jahrb Mineral Geol Palaeontol A*. 2012;189:197–206.
- [129] Serras P, Palomares V, Rojo T, Brand HE, Sharma N. Structural evolution of high energy density $\text{V}(3+)/\text{V}(4+)$ mixed valent $\text{Na}_3\text{V}_2\text{O}_2\text{x}$ ($\text{PO}_4\text{F}_3\text{O}_{2\text{x}}$ ($\text{x} = 0.8$) sodium vanadium fluorophosphate using in situ synchrotron X-ray powder diffraction. *J Mater Chem A*. 2014;2:7766–79.
- [130] Brachtel G, Bukovec N, Hoppe R. Das erste Oxomanganat(III) mit Inselstruktur: zur Kenntnis von $\text{Na}_5(\text{MnO}_4)_2$. *Z Anorg Allg Chem*. 1984;515:101–13.
- [131] Wang H-W, Bish DL. A $\text{P}(\text{H}_2\text{O})$ -dependent structural phase transition in zeolite natrolite. *Am Miner*. 2008;93:1191–4.
- [132] Peacor DR, Bürger MJ. The determination and refinement of the structure of narsarsukite, $\text{Na}_2\text{TiOSi}_4\text{O}_{10}$. *Am Mineral*. 1962;47:539–56.
- [133] Wohlfahrt A. Kristallchemie von verbindungen und mischkristallen mit millarit-struktur. *Heidelb Geowiss Abh*. 1998;92:1–91.
- [134] Zschornak M. 2015. dissertation, TU Bergakademie Freiberg. <http://nbn-resolving.de/urn:nbn:de:bsz:105-qucosa-169703>.
- [135] Thomas LH. The calculation of atomic fields. *Math Proc Cambridge Philos Soc*. 1927;23:542–8.
- [136] Fermi E. Eine statistische methode zur bestimmung einiger eigenschaften des atoms und ihre anwendung auf die theorie des periodischen systems der elemente. *Z Phys*. 1928;48:73–9.
- [137] Slater JC. A simplification of the Hartree-Fock method. *Phys Rev*. 1951;81:385.
- [138] Hohenberg P, Kohn W. Inhomogeneous electron gas. *Phys Rev*. 1964;136:B864.
- [139] Kohn W, Sham LJ. Self-consistent equations including exchange and correlation effects. *Phys Rev*. 1965;140:A1133.
- [140] Johannes MD, Love CT, Swider-Lyons K. Calculations in Li-ion battery materials. In: Breitkopf C, Swider-Lyons K, editors. *Springer Handbook of Electrochemical Energy*. Berlin Heidelberg: Springer; 2016:313–28.
- [141] Jain A, Ong SP, Hautier G, Chen W, Richards WD, Dacek S, et al. Commentary: the materials project: a materials genome approach to accelerating materials innovation. *APL Mater*. 2013;1:011002.
- [142] Jain A, Shin Y, Persson KA. Computational predictions of energy materials using density functional theory. *Nat Rev Mater*. 2016;1:15004.
- [143] Urban A, Seo D-H, Ceder G. Computational understanding of Li-ion batteries. *NPJ Comput Mater*. 2016;2:16002.
- [144] Nørskov JK, Bligaard T, Rossmeisl J, Christensen CH. Towards the computational design of solid catalysts. *Nat Chem*. 2009;1:37–46.
- [145] Sokolov AN, Atahan-Evrenk S, Mondal R, Akkerman HB, Sánchez-Carrera RS, Granados-Focil S, et al. From computational discovery to experimental characterization of a high hole mobility organic crystal. *Nat Commun*. 2011;2:437.
- [146] Pyzer-Knapp EO, Suh C, Gómez-Bombarelli R, Aguilera-Iparraguirre J, Aspuru-Guzik A. What is high-throughput virtual screening? A perspective from organic materials discovery. *Annu Rev Mater Res*. 2015;45:195–216.
- [147] Sanvito S, Oses C, Xue J, Tiwari A, Zic M, et al. Accelerated discovery of new magnets in the Heusler alloy family. *Sci Adv*. 2017;14:e1602241.
- [148] Ong SP, Richards WD, Jain A, Hautier G, Kocher M, Cholia S, et al. Python materials genomics (pymatgen): a robust, open-source python library for materials analysis. *Comput Mater Sci*. 2013;68:314–9.
- [149] Larsen AH, Mortensen JJ, Blomqvist J, Castelli IE, Christensen R, Dułak M, et al. The atomic simulation environment – a Python library for working with atoms. *J Phys Condens Matter*. 2017;29:273002.
- [150] Curtarolo S, Setyawan W, Hart CL, Jahnatek M, Chepulskii RV, Taylor RH, et al. AFLOW: an automatic framework for high-throughput materials discovery. *Comput Mater Sci*. 2012;58:218–226.
- [151] Tarascon J-M, Armand M. Issues and challenges facing rechargeable lithium batteries. *Nature*. 2001;414:359–67.
- [152] Armand M, Tarascon J-M. Building better batteries. *Nature*. 2008;451:652–7.
- [153] Bruce PG, Freunberger SA, Hardwick LJ, Tarascon J-M. Li-O₂ and Li-S batteries with high energy storage. *Nat Mater*. 2012;11:19–29.
- [154] Larcher D, Tarascon J-M. Towards greener and more sustainable batteries for electrical energy storage. *Nat Chem*. 2015;7:19–29.
- [155] Kim S-W, Seo D-H, Ma X, Ceder G, Kang K. Electrode materials for rechargeable sodium-ion batteries: potential alternatives to current lithium-ion batteries. *Adv Energy Mat*. 2012;2:710–21.
- [156] Hautier G, Jain A, Ong SP, Kang B, Moore C, Doe R, Ceder G. Phosphates as lithium-ion battery cathodes: an evaluation based on high-throughput *ab initio* calculations. *Chem Mater*. 2011;23:3495–508.
- [157] Aydinol MK, Kohan AF, Ceder G, Cho K, Joannopoulos J. *Ab initio* study of lithium intercalation in metal oxides and metal dichalcogenides. *Phys Rev B*. 1997;56:1354.
- [158] Perdew JP, Burke K, Ernzerhof M. Generalized gradient approximation made simple. *Phys Rev Lett*. 1997;77:3865.
- [159] Heyd J, Scuseria GE. Hybrid functionals based on a screened Coulomb potential. *J Chem Phys*. 2003;118:8207.
- [160] Anisimov VI, Zaanen J, Andersen OK. Band theory and Mott insulators: Hubbard U instead of Stoner I . *Phys Rev B*. 1991;44:943.
- [161] Kulik HJ, Cococcioni M, Scherlis DA, Marzari N. Density functional theory in transition-metal chemistry: a self-consistent Hubbard U approach. *Phys Rev Lett*. 2006;97:103001.
- [162] Ong SP, Chevrier VL, Ceder G. Comparison of small polaron migration and phase separation in olivine LiMnPO_4 and LiFePO_4 using hybrid density functional theory. *Phys Rev B*. 2011;83:075112.
- [163] Becke AD. Density-functional exchange-energy approximation with correct asymptotic behavior. *Phys Rev A*. 1988;38:3098.
- [164] Lee C, Yang W, Parr RG. Development of the Colle-Salvetti correlation-energy formula into a functional of the electron density. *Phys Rev B*. 1988;37:785.

- [165] Becke AD. Density-functional thermochemistry. III. The role of exact exchange. *J Chem Phys.* 1993;98:5648.
- [166] Adamo C, Barone V. Toward reliable density functional methods without adjustable parameters: the PBEo model. *J Chem Phys.* 1999;110:6158.
- [167] Toumar AJ, Ong SP, Richards WD, Dacek S, Ceder G. Vacancy ordering in O₃-type layered metal oxide sodium-ion battery cathodes. *Phys Rev Appl.* 2015;4:064002.
- [168] Simon P, Gogotsi Y, Dunn B. Where do batteries end and supercapacitors begin? *Science.* 2014;343:1210–1.
- [169] Kang K, Meng YS, Bréger J, Grey CP, Ceder G. Electrodes with high power and high capacity for rechargeable lithium batteries. *Sci.* 2006;311:977–80.
- [170] Whittingham MS. Ultimate limits to intercalation reactions for lithium batteries. *Chem Rev.* 2014;114:11414–43.
- [171] Yabuuchi N, Kubota K, Dahbi M, Komaba S. Research development on sodium-ion batteries. *Chem Rev.* 2014;114:11636–82.
- [172] Canepa P, Gautam GS, Hannah DC, Malik R, Liu M, Gallagher KG, Persson KA, Ceder G. Odyssey of multivalent cathode materials: open questions and future challenges. *Chem Rev.* 2017;117:4287–341.
- [173] Yoo HD, Shterenberg I, Gofer Y, Gershinsky G, Pour N, Aurbach D. Mg rechargeable batteries: an on-going challenge. *Energy Environ Sci.* 2013;6:2265–79.
- [174] Rong Z, Malik R, Canepa P, Gautam GS, Liu M, Jain A, Persson K, Ceder G. Materials design rules for multivalent ion mobility in intercalation structures. *Chem Mater.* 2015;27:6016–21.
- [175] Canepa P, Bo S-H, Gautam GS, Key B, Richards WD, Shi T, et al. High magnesium mobility in ternary spinel chalcogenides. *Nat Commun.* 2017;8:1759.
- [176] Pechukas P. Transition State Theory. *Annu Rev Phys Chem.* 1981;32:159–77.
- [177] Cabrera N, Mott NF. Theory of the oxidation of metals. *Reports on Progress in Physics* 1949;12:163–84.
- [178] Yashima M, Itoh M, Inaguma Y, Morii Y. Crystal Structure and Diffusion Path in the Fast Lithium-Ion Conductor La_{0.62}Li_{0.16}TiO₃. *J Am Chem Soc.* 2005;127:3491–3495.10.1021/ja0449224.
- [179] Sheppard D, Terrel R, Henkelman G. Optimization methods for finding minimum energy paths. *J Chem Phys.* 2008;128:134106.
- [180] Miara LJ, Suzuki N, Richards WD, Wang Y, Kim JC, Ceder G. Li-ion conductivity in Li_xS₃N. *J Mater Chem A.* 2015;3:20338–44.
- [181] Ong SP, Mo Y, Richards WD, Miara L, Lee HS, Ceder G. Phase stability, electrochemical stability and ionic conductivity of the Li_{10±1}MP₂X₁₂ (M = Ge, Si, Sn, Al or P, and X = O, S or Se) family of superionic conductors. *Energy Environ Sci.* 2013;6:148–56.
- [182] Kamaya N, Homma K, Yamakawa Y, Hirayama M, Kanno R, Yonemura M, et al. A lithium superionic conductor. *Nat Mater.* 2011;10:682–686.
- [183] Bron P, Johansson S, Zick K, Schmedt Auf Der Günne J, Dehnen S, Roling B. Li₁₀SnP₂S₁₂: an affordable lithium superionic conductor. *J Am Chem Soc.* 2013;135:15694–7.
- [184] Richards WD, Tsujimura T, Miara LJ, Wang Y, Kim JC, Ong SP, Uechi I, Suzuki N, Ceder G. Design and synthesis of the superionic conductor Na₁₀SnP₂S₁₂. *Nat Commun.* 2016;7:11009.
- [185] Miara LJ, Ong SP, Mo Y, Richards WD, Park Y, Lee J-M, Lee HS, Ceder G. Effect of Rb and Ta doping on the ionic conductivity and stability of the garnet Li_{7+2x-y}(La_{3-x}Rb_x)(Zr_{2-y}Ta_y)O₁₂ (0 ≤ x ≤ 0.375, 0 ≤ y ≤ 1) superionic conductor: a first principles investigation. *Chem Mater.* 2013;25:3048–55.
- [186] Kuhn A, Gerbig O, Zhu C, Falkenberg F, Maier J, Lotsch BV. A new ultrafast superionic Li-conductor: ion dynamics in Li₁₁Si₂PS₁₂ and comparison with other tetragonal LGPS-type electrolytes. *Phys Chem Chem Phys.* 2014;16:14669–74.
- [187] Malik R, Abdellahi A, Ceder G. A critical review of the Li insertion mechanisms in LiFePO₄ electrodes. *J Electrochem Soc.* 2013;160:A3179–97.
- [188] Liu M, Rong Z, Malik R, Canepa P, Jain A, Ceder G, Persson KA. Spinel compounds as multivalent battery cathodes: a systematic evaluation based on *ab initio* calculations. *Energy Environ Sci.* 2015;8:964–74.
- [189] Gautam GS, Canepa P, Abdellahi A, Urban A, Malik R, Ceder G. The intercalation phase diagram of Mg in V₂O₅ from first-principles. *Chem Mater.* 2015;27:3733–42.
- [190] Gautam GS, Canepa P, Malik R, Liu M, Persson K, Ceder G. First-principles evaluation of multi-valent cation insertion into orthorhombic V₂O₅. *Chem Commun.* 2015;51:13619–22.
- [191] Maxisch T, Zhou F, Ceder G. *Ab initio* study of the migration of small polarons in olivine Li_xFePO₄ and their association with lithium ions and vacancies. *Phys Rev B.* 2006;73:104301.
- [192] Xu B, Meng S. Factors affecting Li mobility in spinel LiMn₂O₄ – a first-principles study by GGA and GGA + U methods. *J Power Sources.* 2010;195:4971–6.
- [193] Hannah DC, Gautam GS, Canepa P, Rong Z, Ceder G. Magnesium ion mobility in post-spinels accessible at ambient pressure. *Chem Commun.* 2017;53:5171–4.
- [194] Sun X, Blanc L, Nolis GM, Bonnick P, Cabana J, Nazar LF. NaV_{1.25}Ti_{0.75}O₄: a potential post spinel cathode material for Mg batteries. *Chem Mater.* 2018;30:121–8.
- [195] Mukherjee A, Sa N, Phillips PJ, Burrell A, Vaughney J, Klie RF. Direct Investigation of Mg intercalation into the orthorhombic V₂O₅ cathode using atomic-resolution transmission electron microscopy. *Chem Mater.* 2017;29:2218–26.
- [196] Rong Z, Kichaev D, Canepa P, Huang W, Ceder G. An efficient algorithm for finding the minimum energy path for cation migration in ionic materials. *J Chem Phys.* 2016;145:074112.
- [197] Rong Z, Xiao P, Liu M, Huang W, Hannah DC, Scullin W, Persson KA, Ceder G. Fast Mg²⁺ diffusion in Mo₃(PO₄)₃O for Mg batteries. *Chem Commun.* 2017;53:7998–8001.
- [198] Freysoldt C, Grabowski B, Hückel T, Neugebauer J, Kresse G, Janotti A, Van De Walle CG. First-principles calculations for point defects in solids. *Rev Mod Phys.* 2014;86:253.
- [199] Islam M, Driscoll D, Fisher C, Slater P. Atomic-scale investigation of defects, dopants, and lithium transport in the LiFePO₄ olivine-type battery material. *Chem Mater.* 2005;17:5085–92.
- [200] Morgan D, Van Der Ven A, Ceder G. Li conductivity in LixMPO₄ (M = Mn, Fe, Co, Ni) olivine materials. *Electrochim Solid-State Lett.* 2004;7:A30–2.

- [201] Maragliano L, Vanden-Eijnden E. A temperature accelerated method for sampling free energy and determining reaction pathways in rare events simulations. *Chem Phys Lett.* 2006;426:168–75.
- [202] Laio A, Parrinello M. Escaping free-energy minima. *PNAS.* 2002;99:12562–6.
- [203] Abrams C, Bussi G. Enhanced sampling in molecular dynamics using metadynamics, replica-exchange, and temperature-acceleration. *Entropy.* 2014;16:163–99.
- [204] Boulfelfel SE, Seifert G, Leoni S. Atomistic investigation of Li⁺ diffusion pathways in the olivine LiFePO₄ cathode material. *J Mater Chem.* 2011;21:16365–72.
- [205] Johnston W, Heikes R, Sestrich D. The preparation, crystallography, and magnetic properties of the Li_xCo_(1-x)O system. *J Phys Chem Solids.* 1958;7:1–13.
- [206] Mizushima K, Jones P, Wiseman P, Goodenough JB. Li_xCoO₂ (0 < x < 1): a new cathode material for batteries of high energy density. *Mater Res Bull.* 1980;15:783–9.
- [207] Padhi AK, Nanjundaswamy K, Goodenough JB. Phospho-olivines as positive-electrode materials for rechargeable lithium batteries. *J Electrochem Soc.* 1997;144:1188–94.
- [208] Fuchs JN. Über ein neues mineral (triphylin). *Adv Synth Catal.* 1834;3:98–104.
- [209] Fuchs JN. Vermischte Notizen. *J Prakt Chem.* 1835;5:316–24.
- [210] Björling CO, Westgren A. Minerals of the varuträsk pegmatite: IX. X-ray Studies on triphylite, varulito, and their oxidation products. *Geol Foeren Stockholm Foerh.* 1938;60:67–72.
- [211] Yakubovich OV, Simonov MA, Belov NV. The crystal structure of a synthetic triphylite LiFe[PO₄]. *Sov Phys Dokl.* 1977;22:347.